PLOS GENETICS

RESEARCH ARTICLE

A mutant form of Dmc1 that bypasses the requirement for accessory protein Mei5-Sae3 reveals independent activities of Mei5-Sae3 and Rad51 in Dmc1 filament stability

Diedre Reitz[1], **Jennifer Grubb**[2], **Douglas K. Bishop**[1,2]*

1 Committee on Genetics, Genomics, and Systems Biology, University of Chicago, Chicago, Illinois, United States of America, **2** Department of Radiation and Cellular Oncology, Department of Molecular Genetics and Cell Biology, University of Chicago, Chicago, Illinois, United States of America

* dbishop@uchicago.edu

OPEN ACCESS

Citation: Reitz D, Grubb J, Bishop DK (2019) A mutant form of Dmc1 that bypasses the requirement for accessory protein Mei5-Sae3 reveals independent activities of Mei5-Sae3 and Rad51 in Dmc1 filament stability. PLoS Genet 15 (12): e1008217. https://doi.org/10.1371/journal.pgen.1008217

Editor: Michael Lichten, National Cancer Institute, UNITED STATES

Received: May 22, 2019

Accepted: November 15, 2019

Published: December 2, 2019

Data Availability Statement: All relevant data are within the manuscript and its Supporting Information files.

Funding: This work was supported by NIGMS grant GM50936 and NCATS grant 1UL1TR002389-01 to DKB. DFR was partly supported by the NIH Genetics & Regulation Training Grant (T32 GM07197). The funders had no role in study design, data collection and analysis, decision to publish, or preparation of the manuscript.

Abstract

During meiosis, homologous recombination repairs programmed DNA double-stranded breaks. Meiotic recombination physically links the homologous chromosomes ("homologs"), creating the tension between them that is required for their segregation. The central recombinase in this process is Dmc1. Dmc1's activity is regulated by its accessory factors including the heterodimeric protein Mei5-Sae3 and Rad51. We use a gain-of-function *dmc1* mutant, *dmc1-E157D*, that bypasses Mei5-Sae3 to gain insight into the role of this accessory factor and its relationship to mitotic recombinase Rad51, which also functions as a Dmc1 accessory protein during meiosis. We find that Mei5-Sae3 has a role in filament formation and stability, but not in the bias of recombination partner choice that favors homolog over sister chromatids. Analysis of meiotic recombination intermediates suggests that Mei5-Sae3 and Rad51 function independently in promoting filament stability. In spite of its ability to load onto single-stranded DNA and carry out recombination in the absence of Mei5-Sae3, recombination promoted by the Dmc1 mutant is abnormal in that it forms foci in the absence of DNA breaks, displays unusually high levels of multi-chromatid and intersister joint molecule intermediates, as well as high levels of ectopic recombination products. We use super-resolution microscopy to show that the mutant protein forms longer foci than those formed by wild-type Dmc1. Our data support a model in which longer filaments are more prone to engage in aberrant recombination events, suggesting that filament lengths are normally limited by a regulatory mechanism that functions to prevent recombination-mediated genome rearrangements.

Author summary

During meiosis, two rounds of division follow a single round of DNA replication to create the gametes for biparental reproduction. The first round of division requires that the homologous chromosomes become physically linked to one another to create the tension

Competing interests: The authors have declared that no competing interests exist.

that is necessary for their segregation. This linkage is achieved through DNA recombination between the two homologous chromosomes, followed by resolution of the recombination intermediate into a crossover. Central to this process is the meiosis-specific recombinase Dmc1, and its accessory factors, which provide important regulatory functions to ensure that recombination is accurate, efficient, and occurs predominantly between homologous chromosomes, and not sister chromatids. To gain insight into the regulation of Dmc1 by its accessory factors, we mutated Dmc1 such that it was no longer dependent on its accessory factor Mei5-Sae3. Our analysis reveals that Dmc1 accessory factors Mei5-Sae3 and Rad51 have independent roles in stabilizing Dmc1 filaments. Furthermore, we find that although Rad51 is required for promoting recombination between homologous chromosomes, Mei5-Sae3 is not. Lastly, we show that our Dmc1 mutant forms abnormally long filaments, and high levels of aberrant recombination intermediates and products. These findings suggest that filaments are actively maintained at short lengths to prevent deleterious genome rearrangements.

Introduction

Homologous recombination (HR) is a high-fidelity mechanism of repair of DNA double strand breaks (DSBs), interstrand cross-links, and stalled or collapsed replication forks in mitotically dividing cells. In addition, during meiosis, most eukaryotes rely on reciprocal crossover recombination (CO) to physically link the maternal and paternal chromosomes via chiasmata, thereby making it possible for the meiosis I (MI) spindle to create the tension between homolog pairs that is required for their reductional segregation [1]. The RecA homolog Dmc1 is specifically expressed in meiotic cells and plays the central catalytic role in meiotic recombination in budding yeast [2,3]. A second RecA homolog, Rad51, plays the central catalytic role in mitotic recombination [4,5], but is converted to an accessory protein that regulates Dmc1's catalytic activity in meiotic cells [3].

Meiotic recombination is initiated by programmed DSBs formed by the activity of the transesterase Spo11 [6]. Following meiotic DSB formation and end resection, Dmc1 forms a helical nucleoprotein filament on the single-stranded DNA (ssDNA) tracts created by the resection machinery [7]. The nucleoprotein filament then searches the genome for a sequence of duplex DNA that is homologous to the ssDNA onto which it is loaded [8]. This region of homology can be an allelic site on one of the two homologous chromatids or on the sister chromatid. In addition, if a DSB is in a region that is repeated at more than one chromosomal locus, this can result in ectopic recombination between the two chromosomal loci [9–12]. Meiotic recombination normally favors the use of the homologous chromosome rather than the sister chromatid, consistent with the biological requirement for interhomolog (IH) COs for reductional segregation; this phenomenon is known as "IH bias" [13,14]. Once a homologous region of double-stranded DNA (dsDNA) is found, strand exchange occurs to form a tract of hybrid DNA, pairing the ssDNA with the complementary strand of the duplex. Hybrid DNA formation displaces the opposite strand of the donor dsDNA, forming a displacement loop (D-loop) [15]. The repair process then uses the intact donor duplex DNA as a template to direct recombination-associated DNA synthesis [16]. Processing of extended D-loops by helicases gives rise to non-crossover recombinants by a pathway referred to as synthesis-dependent strand annealing [17–19]. The subset of D-loops destined to become COs are stabilized to form a joint molecule (JM) species that can be detected on two-dimensional (2D) gels as a so-called single-end invasion (SEI) [20]. SEIs are then converted to double Holliday Junction

intermediates (dHJs) by the capture of the second end of the DSB and further repair synthesis to generate full length dsDNA [21]. Finally dHJs are resolved by Exo1 and the MutLγ complex to give rise to COs [22].

HR is highly regulated to ensure its accuracy and avoid potentially deleterious consequences of the process. Two key steps in HR, nucleoprotein filament formation and the initial invasion event, are reversible and therefore subject to this regulation [23]. Nucleoprotein filament formation, or nucleation, involves the recruitment of the strand exchange protein to sites of ssDNA tracts, followed by displacement of the high affinity ssDNA binding protein RPA. Next, filaments elongate in a process that is driven by cooperative interactions between strand exchange protomers. A class of accessory proteins collectively referred to as "mediator" proteins can act to promote the displacement of RPA and/or to stabilize nascent filaments, allowing them to elongate [24,25]. Mutants lacking one of these assembly proteins display defects in formation of filaments on ssDNA, which can be detected by immunostaining or other cytological methods following DNA damaging treatment, or during the normal meiotic program. UvrD family helicases, including UvrD in prokaryotes and Srs2 in budding yeast, antagonize recombination at this step by disassembling ssDNA nucleoprotein filaments [26–29]. Though the strippase function of Srs2 with respect to Rad51 filaments has been well documented, Srs2 does not disassemble Dmc1 filaments, and in fact Dmc1 may inhibit Srs2 activity on ssDNA [30,31]. It is currently unknown whether there exists an ssDNA "strippase" that acts on Dmc1.

Under normal circumstances *in vivo*, RecA family proteins form nucleoprotein filaments that are shorter than the resolution limit of conventional light microscopy (~200 nanometers). This is true for RecA, and for both eukaryotic RecA homologs, Rad51 and Dmc1 [32–35]. Super-resolution microscopy imaging of Dmc1 filaments formed during meiosis indicates that Dmc1 filaments are typically about 120 nanometers (nm) long, a length that corresponds to roughly 100 nucleotides when taking into account the fact that RecA family proteins stretch the DNA ~1.5 fold when assembled into a filament [36,37]. Furthermore, in the *exo1-D173A* mutant, in which DNA end resection is impaired during meiosis, JMs are formed at a level that is equivalent to wild-type, implying that short ssDNA tracts support normal meiotic recombination [38]. In contrast, longer than normal Dmc1 filaments accumulate in the absence of Mnd1, a Dmc1 accessory protein that is required for Dmc1 activity after the filament formation stage [36]. Taken together, these results suggest that while RecA family proteins are competent to form long filaments, they are regulated such that they form relatively short filaments *in vivo*. The significance of this regulation and the factors that influence filament length are presently not well understood.

RecA family recombinases are DNA-dependent ATPases, but their ATPase activity is not required for filament formation or for stand exchange [39–42]. Instead, ATP binding changes the conformation of the protein to a form that has high affinity for DNA, and is thus the active form [39,43]. The ADP bound form of the protein has lower affinity for DNA than the ATP-bound form, and is inactive in homology search and strand exchange. In prokaryotes, RecA ATP hydrolysis is required for filament disassembly following strand exchange, or when the protein inappropriately assembles on dsDNA [35,42]. In contrast to RecA, the eukaryotic recombinases Rad51 and Dmc1 display relatively weak intrinsic ATPase activity and rely on Rad54 family ATP-dependent dsDNA translocases to promote their dissociation [44–48]. Translocase driven dissociation is required to clear strand exchange proteins from D-loops to allow completion of recombination events [49]. Translocases also prevent accumulation of off-pathway complexes formed by filament nucleation on unbroken dsDNA [47,49–53]. A previous study of human Rad51 used *in vitro* single-molecule fluorescence imaging to show that Rad51-ADP dissociation from dsDNA is inefficient and incomplete, suggesting that the activity of the translocases is required even when Rad51 is in the ADP-bound form [54]. Moreover,

Rad54 overexpression was observed to suppress the defects associated with Rad51-K191R, a *rad51* mutant that is completely defective in ATP hydrolysis, implying that the ATPase activity of Rad51 is not required for it to be removed from dsDNA by Rad54 [55–57]. Finally, in the context of the nucleoprotein filament, the ATPase domain of one protomer directly contacts the N-terminal binding domain of the adjacent protomer; this observation is believed to be the structural basis for the finding that ATP-binding promotes protomer-protomer cooperativity [58,59].

We are interested in understanding how accessory proteins regulate the activity of the meiotic RecA homolog Dmc1. In *Saccharomyces cerevisiae*, Dmc1's activity is regulated by at least five key accessory proteins including RPA, Mei5-Sae3, Hop2-Mnd1, Rad51, and the translocase Rdh54 (a.k.a. Tid1). RPA rapidly binds to tracts of ssDNA and serves to coordinate the interactions between Dmc1's other accessory proteins and ssDNA [60]. *In vivo*, Mei5-Sae3 and Rad51 are required for normal Dmc1 filament formation at tracts of RPA coated ssDNA, suggesting that these factors are involved in nucleation and/or filament elongation [61–63]. Conversely, Hop2-Mnd1 is required for strand exchange, but not for filament nucleation or stability [64,65]. Rdh54 is a Rad54 family translocase implicated in promoting dissociation of Dmc1 from dsDNA, as discussed above.

Budding yeast Mei5-Sae3 is a homolog of *Schizosaccharomyces pombe* and mammalian Sfr1-Swi5/MEI5-SWI5, with no known homolog in plants [66]. In budding yeast, Mei5-Sae3 is Dmc1-specific, whereas in fission yeast Sfr1-Swi5 is an accessory factor to both Dmc1 and Rad51 [67]. In mammals, MEI5-SWI5 protein is reported to function with RAD51, but there is no known interaction with DMC1, and an effort to detect DMC1 stimulatory activity *in vitro* yielded negative results [68,69]. Biochemical studies have suggested several functions for Mei5-Sae3. First, studies using fission yeast proteins have shown that Sfr1-Swi5 stimulates fission yeast Rad51 (referred to as Rhp51) and Dmc1 in three-stranded DNA exchange reactions, and it helps Rhp51 overcome the inhibitory effect of RPA [67]. Studies using purified budding yeast Mei5-Sae3 and Dmc1 similarly concluded that Mei5-Sae3 promotes Dmc1 loading onto RPA-coated ssDNA, and that it enhances Dmc1-mediated D-loop formation when used alone, or in combination with Rad51 [3,60,70]. In addition to this mediator activity, Haruta et al. also reported that Sfr1-Swi5 enhances Rhp51's ATPase activity; this result was subsequently confirmed and extended by work from Su et al. using purified *Mus musculus* proteins [67,69]. Su et al. showed that SWI5-MEI5 stimulates RAD51 by promoting ADP release, the step in ATP hydrolysis that is believed to be the slowest and thus rate-limiting [69,71]. Enhancement of ADP release is thought to have a stabilizing effect on Rad51 filaments by maintaining them in the ATP-bound state. In addition, later studies using single-molecule fluorescence resonance energy transfer, concluded that mouse SWI5-MEI5 promotes RAD51 nucleation by preventing dissociation, effectively reducing the number of protomers required for a nucleation event from three to two [72]. The same study also found that fission yeast Sfr1-Swi5 prevents Rhp51 disassembly, suggesting a conserved role for this complex in stabilizing Rad51 filaments.

In vivo, *Saccharomyces cerevisiae* Dmc1 and Mei5-Sae3 are interdependent for focus formation, and the foci formed by the two proteins co-localize with one another, and with other DSB-dependent proteins such as Rad51 [62,63]. Moreover, Dmc1 and Mei5-Sae3 both depend on Rad51 for normal meiotic focus formation; average focus staining intensity is lower in *rad51* mutants than in wild-type [61,62]. Consistent with it being necessary for Dmc1 focus formation, Mei5-Sae3 is also required for Dmc1-mediated recombination. *In vivo*, DSBs form normally in *mei5* or *sae3* mutants, but these intermediates are not converted to dHJs [62,63,73]. Fission yeast Rhp51 differs from Dmc1 in its dependency on Sfr1-Swi5; while loss of Sfr1-Swi5 reduces recombination, recombination is only eliminated when both Sfr1-Swi5 and Rhp55-Rhp57, a heterodimeric accessory protein homologous to budding yeast

Rad55-Rad57, are deleted [74]. Similarly, knockdown of MEI5-SWI5 in human cells impairs RAD51 focus formation in response to ionizing radiation and also reduces recombination [68]. In contrast, deletion of mouse *Swi5* and *Sfr1* does not reduce the level of recombination when assayed with a direct-repeat reporter construct, but it does make cells more sensitive to DNA damaging agents that require HR for repair, including ionizing radiation, camptothecin, and poly(ADP-ribose) polymerase (PARP) inhibitor [75]. It is not known whether these differences in the requirement of SWI5-MEI5 by RAD51 in humans and mouse are due to differences in the cell types used or true biological differences in the human and mouse RAD51 recombinases [68].

Rad51, the RecA homolog that catalyzes homology search and strand exchange during mitotic recombination, is the second accessory protein that plays a role in forming wild-type Dmc1 filaments during meiosis [61]. Although Rad51 is required for normal meiotic recombination, its strand exchange activity is dispensable [3]. In fact, Rad51 strand exchange activity is inhibited during MI by the meiosis-specific protein Hed1 [76,77]. In the absence of Rad51, Dmc1 foci have reduced staining intensity, suggesting that filaments are defective [61,78]. Recombination still occurs in *rad51* mutants, but it is mis-regulated such that dHJs form predominantly between sister chromatids, instead of between homologous chromosomes [79]. In addition, CO formation is reduced, only a sub-population progresses through meiotic divisions, and the spores formed are not viable [4]. In biochemical reconstitution experiments, Rad51 alone can stimulate Dmc1-mediated D-loop formation, although optimal levels of D-loop formation require both Rad51 and Mei5-Sae3 [3]. In spite of its importance as a Dmc1 accessory factor, very little is known about the molecular mechanisms involved in Rad51's non-catalytic role in meiotic recombination.

One approach to studying the role of accessory proteins is to assume that the activity of the enzyme has evolved to depend on that accessory factor. In this view, beneficial regulation of an enzyme's activity is selected for at the expense of the enzyme's intrinsic activity. If such an evolutionary process is responsible for a particular regulatory mechanism, it should be possible to mutate the core enzyme to eliminate the "built-in" defect, rendering the mutant protein capable of catalyzing its reaction in the absence of the accessory protein. Comparison of the activities of the mutant and wild-type proteins with and without the accessory protein can then provide mechanistic insight into the processes that accessory protein normally regulates.

We applied this approach to Dmc1 in an attempt to further elucidate the mechanisms through which Mei5-Sae3 influences Dmc1's activity. We identified a gain-of-function *dmc1* mutant whose activity is independent of Mei5-Sae3. Characterization of this Dmc1 mutant provides new insight into the mechanism of action of Mei5-Sae3 *in vivo*, and also sheds light on the functional relationship between Mei5-Sae3 and Rad51. Furthermore, characterization of this gain-of-function version of Dmc1 reveals that it forms longer than normal filaments and displays higher than normal levels of IS, ectopic, and multi-chromatid recombination. We interpret these observations in the context of recent studies showing that a single strand exchange filament can simultaneously engage more than one dsDNA molecule.

Results

In order to better understand the function of Mei5-Sae3 and Rad51 in Dmc1-mediated HR, we sought to identify a *DMC1* allele that would bypass the requirement for one of these accessory factors. Analysis of Dmc1-mediated recombination in the absence of an accessory factor would then allow us to identify regulatory features that depend on the accessory protein by comparison to the wild-type process. To this end, we constructed two *dmc1* mutants based on previously characterized gain-of-function mutations in Dmc1 homologs, RecA-E96D and

Table 1. Spore viabilities for strains in study. p-values are reported for z-scores using a two-proportion z-score test [82]. Comparison for single mutants is to wild-type. Comparison for double mutants is to each of the single mutants (for example, *dmc1-E157D sae3* is compared to *dmc1-E157D*). Comparison for heterozygotes is to homozygotes.

Strain	n (tetrads)	Spore viability (%)	p-value (two-proportion z-score)
wild-type	153	98.4	N.A.
dmc1-E157D	215	57.6	$p < 0.01$
mei5	no tetrads formed	N.A.	N.A.
rad51	40	<0.6	N.A.
rad51-II3A	19	82.9	$p < 0.01$
rdh54	40	91.9	$p < 0.01$
dmc1-E157D mei5	267	50.3	$p < 0.01$
dmc1-E157D rad51	34	0.7	N.A.
dmc1-E157D rad51-II3A	22	17.0	$p < 0.01$
dmc1-E157D rdh54	no tetrads formed	N.A.	N.A.
dmc1-E157D sae3	39	57.0	$p = 0.4$ (not significant)
dmc1-E157D mei5 rad51	no tetrads formed	N.A.	N.A.
DMC1$^+$/dmc1-E157D	47	91.2	$p < 0.01$
DMC1$^+$/dmc1-E157D mei5/"	69	58.8	$p < 0.01$

N.A. = not applicable; for samples that do not meet the success/failure condition for z-scores and wild-type to itself. Strains used in experiments in the order in which they appear in table, top to bottom: DKB3698, DKB6320, DKB3710, DKB3689, DKB2526, DKB6342, DKB6299, DKB6300, DKB6539, DKB6540, DKB6393, DKB6400, DKB6583, DKB6412, DKB6413, DKB6525, DKB6619, DKB6406, DKB6407.

https://doi.org/10.1371/journal.pgen.1008217.t001

Rad51-I345T [42,80,81]. Sequence alignments indicated that the amino acid residues altered in RecA-E96D and Rad54-I145T mutants are conserved allowing us to construct corresponding mutant forms of Dmc1; for RecA-E96D the corresponding mutant is Dmc1-E157D and for Rad51-I134T the corresponding mutant is Dmc1-I282T. The RecA-E96D mutation shortens the length of a critical amino acid side chain in the ATPase active site, increasing the distance between the water molecule that acts as the nucleophile for hydrolysis and the activating carboxylate [80]. The mutation dramatically reduces the rate of ATP hydrolysis thereby maintaining RecA in the ATP-bound form, which is active for DNA binding, homology search, and strand exchange. Due to the high sequence conservation of this site, Dmc1-E157D is very likely to be defective in ATPase activity, like RecA-E96D. The Rad51-I345T mutation suppresses defects conferred by the heterodimeric accessory protein Rad55-Rad57, which stabilizes Rad51 filaments [81]; we reasoned that the corresponding mutation in Dmc1 might suppress the requirement for Mei5-Sae3 as biochemical studies on Swi5-Sfr1, which is homologous to Mei5-Sae3, indicated Swi5-Sfr1 also acts by stabilizing strand exchange filaments [67,74].

To assess whether either of these Dmc1 mutants would bypass Mei5-Sae3 and/or Rad51, we constructed diploid yeast lacking either Mei5 or Rad51 with the corresponding Dmc1 mutation, and assessed sporulation efficiency and spore viability alongside *DMC1$^+$ mei5* and *DMC1$^+$ rad51* controls. In a *mei5* strain, tetrads are formed very inefficiently, whereas in a *rad51* mutant, tetrads are formed, but almost all spores within them are dead [4,62,63]. We found that *dmc1-E157D* bypasses Mei5-Sae3 with respect to sporulation and spore viability (Table 1). The spore viabilities of *dmc1-E157D*, *dmc1-E157D mei5*, and *dmc1-E157D sae3* are nearly identical to one another (57.6%, 50.3%, and 57.0% respectively), suggesting that Dmc1-E157D function is largely independent of Mei5-Sae3. In contrast, *dmc1-E157D* does not bypass the requirement for *rad51* with respect to spore viability (<0.6% in *rad51* versus 0.7% in *dmc1-E157D rad51*).

Spore viability data from a *dmc1-E157D/DMC1*$^{+}$ *mei5/mei5* heterozygote indicates that Dmc1-E157D is dominant to wild-type Dmc1 (Dmc1-WT) with respect to formation of viable spores in a *mei5* mutant background (58.8% in *dmc1-E157D/DMC1*$^{+}$ *mei5/mei5*, vs. 50.3% in *dmc1-E157D/dmc1-E157D mei5/mei5)*. In contrast, Dmc1-E157D causes only a minor reduction in spore viability when both Dmc1-WT and Mei5 proteins are present (91.2% in *dmc1-E157D/DMC1+ MEI5+/MEI5+* vs. 98.4% in WT). In contrast to *dmc1-E157D*, we did not detect phenotypic suppression in *dmc1-I282T* mutants, either with respect to prophase arrest in a *mei5* mutant background, or with respect to spore viability in a *rad51* background. Importantly, the Dmc1-E157D mutation does not result in increased expression or stability of the protein as assayed by Western blotting of meiotic yeast whole cell extracts, thus ruling out a trivial explanation for Dmc1-E157D's bypass of the *mei5* and *sae3* mutations (S1 Fig).

Dmc1-E157D forms meiotic immunostaining foci in the absence of Mei5 and Rad51

We next performed immunofluorescence staining of spread meiotic nuclei to examine Dmc1 focus formation in the *dmc1-E157D* and *dmc1-E157D mei5* strains. As shown previously, meiotic Dmc1-WT focus formation is severely defective in *mei5* mutant cells, but Dmc1-E157D forms bright foci in the *mei5* mutant background (Fig 1A) [62,63]. Notably, Dmc1 foci accumulate to higher levels and persist for longer in *dmc1-E157D* and *dmc1-E157D mei5* when compared to wild-type (Fig 1B).

One model suggests that Mei5-Sae3 and Rad51 cooperate to promote Dmc1 filament formation [14]. Because *dmc1-E157D* bypasses *mei5*, we reasoned that if this model is correct, *dmc1-E157D* might also bypass the defect seen for formation of brightly-staining Dmc1 foci in *rad51* cells, even though it does not suppress the spore viability defect observed in these cells. To test this, we constructed *dmc1-E157D rad51* and *dmc1-E157D mei5 rad51* strains, and looked for Dmc1 focus formation in spread meiotic nuclei. In contrast to a *rad51* single mutant, in which Dmc1-WT staining intensity is reduced, the Dmc1 foci observed in *dmc1-E157D rad51* and *dmc1-E157D mei5 rad51* nuclei were brighter and more numerous than those in wild-type (Fig 1C and 1D) [61,78]. We conclude that *dmc1-E157D* appears to bypass the role of Rad51 with respect to Dmc1 focus formation.

dmc1-E157D forms immunostaining foci in the absence of DSBs

Because the Dmc1-E157D mutant is modeled after RecA-E96D, which has been shown to form foci on undamaged DNA, we wanted to ask whether the same was true of the corresponding Dmc1 mutant [35]. To determine whether any of the foci that we observed in the *dmc1-E157D* background resulted from binding to chromosomes independent of DSBs, we introduced the *spo11* mutation into our *dmc1-E157D* strains to block DSB formation. Spo11 is the catalytic subunit of a meiosis-specific complex that induces DSBs at the outset of meiosis [6]. Immunostaining of spread meiotic nuclei for Dmc1 and RPA revealed that in contrast to the *spo11* single mutant, which typically forms few if any Dmc1 foci, nearly all *spo11 dmc1-E157D* nuclei contained numerous Dmc1 foci (Fig 1C and 1E) [51]. RPA serves as a marker for DSB-associated tracts of ssDNA in mid-to-late prophase I. RPA foci are detected early in prophase in *spo11* mutants owing to the role of RPA in pre-meiotic DNA replication, but then disappear 4 hours after induction of meiosis [83]. We found that at 4 hours, the majority of nuclei lacking RPA foci contained Dmc1 foci in *spo11 dmc1-E157D* and *spo11 dmc1-E157D mei5* (100% and 96% of nuclei lacking RPA had Dmc1 foci, respectively) (Fig 1E) indicating that Dmc1-E157D forms DSB-independent foci. It is thus likely that a substantial fraction of the foci observed in *SPO11*$^{+}$ *dmc1-E157D* cells represent off-pathway structures

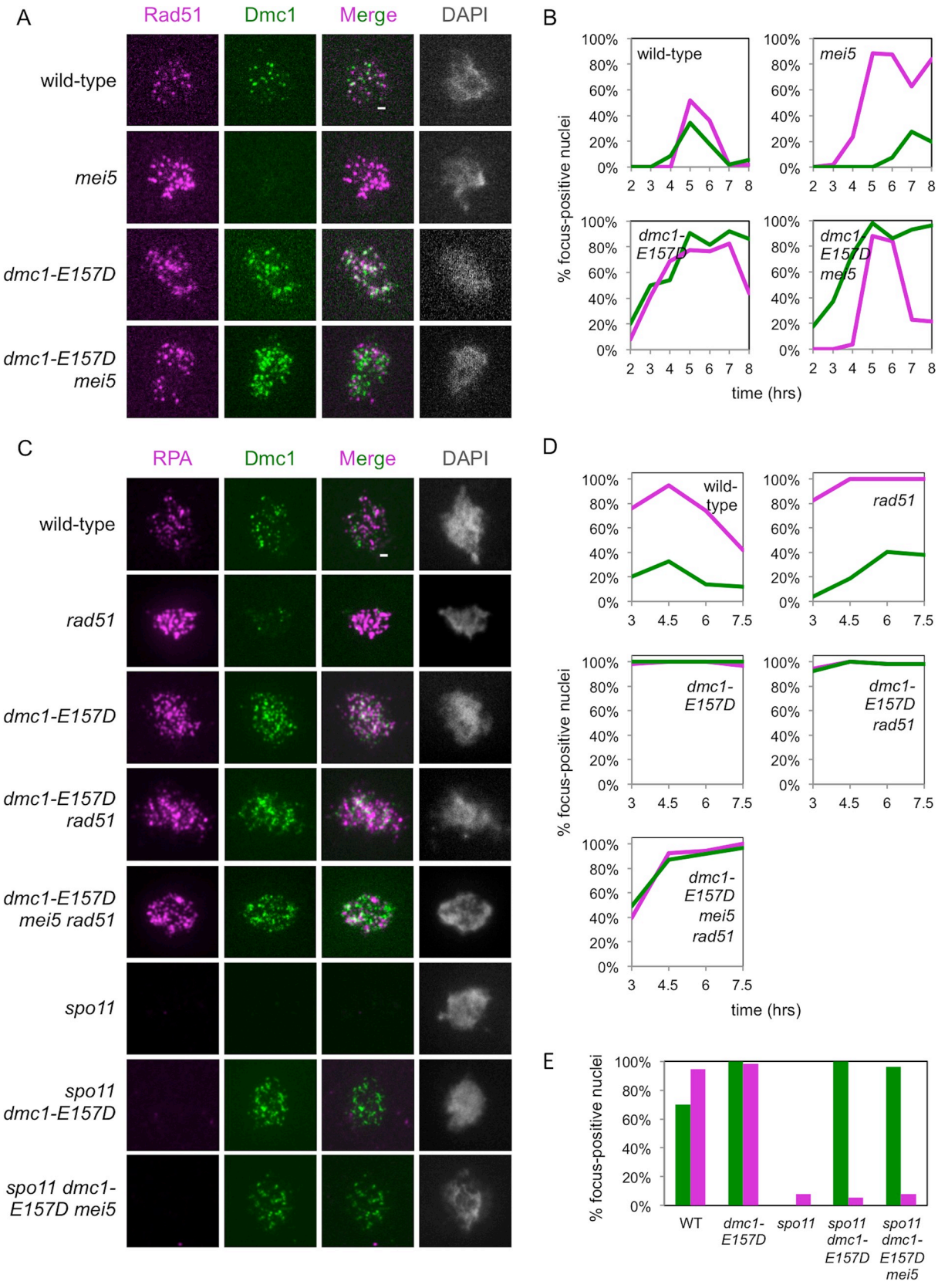
A
Rad51
Dmc1
Merge
DAPI
wild-type
mei5
dmc1-E157D
dmc1-E157D mei5
B
wild-type
mei5
dmc1-E157D
dmc1-E157D mei5
% focus-positive nuclei
time (hrs)
C
RPA
Dmc1
Merge
DAPI
wild-type
rad51
dmc1-E157D
dmc1-E157D rad51
dmc1-E157D mei5 rad51
spo11
spo11 dmc1-E157D
spo11 dmc1-E157D mei5
D
wild-type
rad51
dmc1-E157D
dmc1-E157D rad51
dmc1-E157D mei5 rad51
% focus-positive nuclei
time (hrs)
E
% focus-positive nuclei
WT
dmc1-E157D
spo11
spo11 dmc1-E157D
spo11 dmc1-E157D mei5

Fig 1. *dmc1-E157D* bypasses *mei5*, *rad51* with respect to focus formation. (a, c) Representative wide-field microscopy imaging of spread meiotic nuclei are shown for each strain. Scale bars represent 1 μm. (b, d) Quantitation. Nuclei were scored as focus positive if they contained three or more foci of a given type. Dmc1 (green), Rad51 or RPA (magenta). (e) Quantitation of *spo11* strains and controls at 4 hours. Strains used in experiments in the order in which they appear in figure, top to bottom: DKB3698, DKB6320, DKB6342, DKB6300, DKB3710, DKB6393, DKB6412.

https://doi.org/10.1371/journal.pgen.1008217.g001

formed by binding unbroken chromosomal loci. However, an increase in the total number of DSBs formed or an increase in DSB lifespan could also partially account for the increased number of Dmc1 foci and their persistence in the *dmc1-E157D* background relative to wild-type.

dmc1-E157D bypasses Mei5, but not Rad51, with respect to meiotic CO formation

To examine whether Dmc1-E157D is competent to carry out recombination in the absence of Mei5, we performed one-dimensional (1D) gel electrophoresis, followed by Southern blotting, to examine DSBs and CO products at the well-characterized recombination hotspot *HIS4*::*LEU2* [84]. XhoI digestion of genomic DNA from meiotic time course experiments followed by 1D gel electrophoresis and Southern blotting to detect the *HIS4*::*LEU2* hotspot can be used to detect DSB intermediates and IH CO products, as well as products that result from ectopic recombination between the *HIS4*::*LEU2* locus and the native *LEU2* locus, which are separated by ~23 kilobases on chromosome III [12,84]. As shown previously, DSBs accumulate and CO formation is very limited in $DMC1^{+}$ *mei5* (Fig 2A and 2B) [62,63]. In contrast, although *dmc1-E157D* and *dmc1-E157D mei5* cells initially accumulate DSBs (Fig 2A and 2B, S2 Fig), those breaks are resolved by 24 hours, at which point CO formation is equivalent to wild-type. Further examination of DSB formation in wild-type and *dmc1-E157D* cells using PstI digestion of genomic DNA from meiotic samples to look at DSB resection status revealed that although DSBs accumulate to somewhat higher levels in *dmc1-E157D* relative to wild-type, there are little or no differences in resection status between the two strains (S2 Fig). Interestingly, ectopic recombination is elevated ~3.5-fold in *dmc1-E157D* and *dmc1-E157D mei5* relative to wild-type. In addition, whereas only 8.7% of $DMC1^{+}$ *mei5* cells progress through a meiotic division, 50.0% of *dmc1-E157D mei5* cells progress, a level nearly equivalent to *dmc1-E157D* (58.4%) (Fig 2B). These results show that Dmc1-E157D bypasses the normal requirement for Mei5 during meiotic recombination.

Because Dmc1-E157D also bypasses Rad51 with respect to forming brightly staining Dmc1 foci, we wanted to ask whether it similarly bypasses Rad51 for CO formation and DSB resolution at *HIS4*::*LEU2*. Previous studies of *rad51* mutants showed that DSBs accumulate and undergo more extensive resection than wild-type [4]. In addition, the final level of COs that form in *rad51* was reported to be 5-fold lower than wild-type, and ectopic recombination is ~1.6-fold higher at 10 hours in sporulation medium [4,85]. We confirmed these phenotypes for the *rad51* single mutant (Fig 2A and 2B). Consistent with the failure of *dmc1-E157D* to rescue the low spore viability phenotype of *rad51* (Table 1), we found that *dmc1-E157D rad51* accumulates hyper-resected DSBs (Fig 2A). Surprisingly, *dmc1-E157D rad51* makes fewer COs than *rad51*, implying that the *dmc1-E157D rad51* double mutant is more defective than either the *dmc1-E157D* or the *rad51* single mutants. Meiotic progression data similarly indicate that *dmc1-E157D rad51* is more defective than both *dmc1-E157D* and *rad51*; only 24.8% of *dmc1-E157D rad51* cells execute at least one meiotic division, compared to 58.4% and 54.5% of *dmc1-E157D* and *rad51* cells, respectively (Fig 2B). Additionally, very little ectopic recombination is detected in *dmc1-E157D rad51*, possibly reflecting the fact that there is less

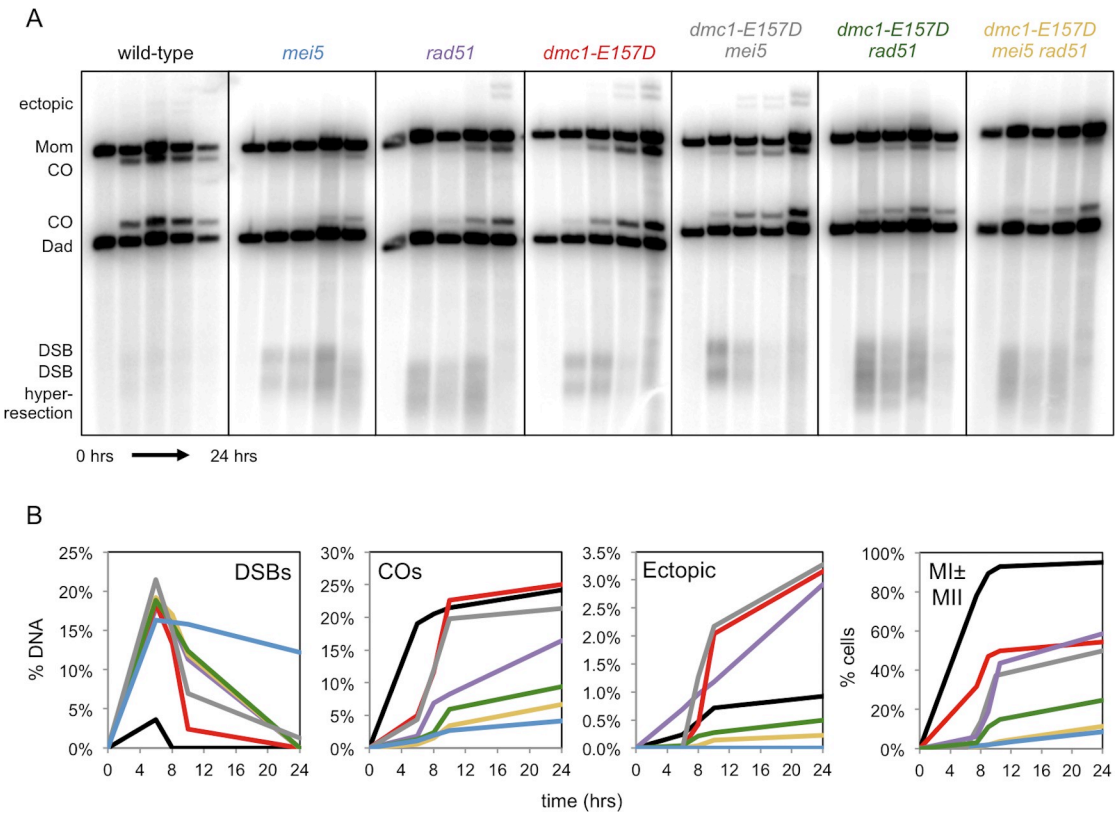

Fig 2. *dmc1-E157D* bypasses *mei5* but not *rad51* with respect to CO formation. (a) Southern blot analysis at the *HIS4*::*LEU2* hotspot following digestion of genomic DNA from meiotic time course experiments with XhoI. Time points shown from left to right are: 0h, 6h, 8h, 10h, 24h. (b) Quantitation of 1D gels shown in (a) and meiotic progression data; black–wild-type, light blue–*mei5*, purple–*rad51*, red–*dmc1-E157D*, gray–*dmc1-E157D mei5*, green–*dmc1-E157D rad51*, yellow–*dmc1-E157D mei5 rad51*. To score meiotic progression, ≥50 cells were scored per time point. Strains used in experiments in the order in which they appear in figure, left to right: DKB3698, DKB6320, DKB3710, DKB6342, DKB6300, DKB6393, DKB6412.

https://doi.org/10.1371/journal.pgen.1008217.g002

recombination overall, or indicating that there is a change in the pattern of JM formation or their resolution. Overall our results indicate that *dmc1-E157D* does not bypass *rad51* with respect to resolution of meiotic DSBs.

The *dmc1-E157D mei5 rad51* triple mutant was similar to the *dmc1-E157D rad51* double mutant, with the triple mutant displaying slightly more pronounced defects in final CO levels (Fig 2A and 2B). We also found that the efficiency of the first meiotic division is somewhat reduced in the *dmc1-E157D mei5 rad51* mutant (11.3%) compared to the *dmc1-E157D rad51* (24.8%) mutant (Fig 2B). These results indicate that recombination in *dmc1-E157D* displays a strong dependence on Rad51, but very limited dependence on Mei5 unless Rad51 is absent.

spo11 rescues the meiotic progression and segregation defects associated with *dmc1-E157D*

In contrast to the typical MI segregation that is observed in wild-type cells, in which there are two well-defined and equally-sized DAPI staining bodies, MI segregation in *dmc1-E157D* often appears to be abnormal, and can include defects such as a single elongated DAPI staining body rather than two separated bodies, as well as separated DAPI staining bodies of dramatically different sizes (S3 Fig). Introduction of the *spo11* mutation into the *dmc1-E157D* background largely rescued these deficiencies. In addition, the *spo11* mutation suppressed the MI

division delay that occurs in *dmc1-E157D* cells (S3 Fig). Thus the meiotic segregation and progression defects observed in the *dmc1-E157D* background are DSB-dependent. This finding suggests that although there are likely numerous DSB-independent Dmc1 foci in these strains, these Dmc1-dsDNA complexes do not dramatically interfere with chromosome segregation.

Dmc1-mediated meiotic recombination is independent of Mei5-Sae3 in *dmc1-E157D*

We next sought to further characterize Dmc1-E157D-mediated recombination in the absence of Mei5 by 2D gel electrophoresis and Southern blotting. Using this method, an array of JM recombination intermediates can be detected at the *HIS4*::*LEU2* locus, including SEIs, intersister-dHJs (IS-dHJs), IH-dHJs, and multi-chromatid JMs (mcJMs) (Fig 3A) [86]. As expected, JM formation is severely compromised in *mei5* (Fig 3B and 3C). In contrast, in *dmc1-E157D mei5*, JM formation is efficient, with IH-dHJ levels equivalent to those in wild-type. IS-dHJs, however, are increased ~3-fold, reducing the IH-dHJ/IS-dHJ ratio from 5.0 in wild-type to ~1.5 in *dmc1-E157D* (Fig 3C). *dmc1-E157D mei5* phenocopies *dmc1-E157D*, also having increased IS-dHJs and a reduced IH/IS ratio of ~1.6. SEIs form at the similar levels in the *dmc1-E157D* and *dmc1-E157D mei5* mutants as in wild-type (Fig 3C). Like IS-dHJs, mcJMs are increased relative to wild-type in both *dmc1-E157D* and *dmc1-E157D mei5* (3.0-fold and 2.7-fold respectively). The similar array of JMs observed in *dmc1-E157D* and *dmc1-E157D mei5* cells further indicates that Dmc1-E157D-mediated recombination occurs independent of Mei5-Sae3. Although a decrease in the IH/IS ratio can be interpreted as a defect in the mechanism of IH bias, this case is unusual in that the decreased ratio results from increased IS-dHJs, with no reciprocal decrease in IH-dHJs. The fact that the level of IH-dHJs in *dmc1-E157D mei5* cells is equivalent to that in wild-type suggests that the mechanism of homolog bias is intact in this mutant, and reveals that Mei5-Sae3 is not required for IH bias. The data also suggest that the *dmc1-E157D* mutant is hyper-recombinant, displaying higher than normal levels of IS-dHJs and mcJMs (Fig 3C), as well as increased ectopic COs (Fig 2B).

The *ndt80* mutation increases total JMs, but does not change their distribution

To rule out the possibility that certain JM species have longer lifespans in the *dmc1-E157D* background, we introduced the *ndt80* mutation. Deletion of *NDT80*$^{+}$ prevents recombination intermediate processing, and JMs accumulate to high levels in this background (S4 Fig) [19]. Importantly, we found that IS-dHJs and mcJMs are also elevated in *ndt80 dmc1-E157D* relative to *ndt80*, with no appreciable differences in SEIs and IH-dHJs (S4 Fig). These findings support a model in which the elevated levels of IS-dHJS and mcJMs are a result of increased formation of these species by Dmc1-E157D, as opposed to these species being less efficiently resolved in *dmc1-E157D* and *dmc1-E157D mei5* cells.

dmc1-E157D rad51 exhibits a profound IH bias defect and a reduction in JM formation

We next examined Dmc1-E157D-mediated recombination in the absence of Rad51 using 2D gel electrophoresis. In a *rad51* mutant, Dmc1 carries out recombination, but there is a profound IH bias defect, and most recombination occurs between sisters [79]. The IH-dHJ/IS-dHJ ratio in *rad51* is 0.4 and the same ratio is observed for *dmc1-E157D rad51* (Fig 3D and 3E, S5 Fig). This defect in the IH/IS ratio is the result of increased IS-dHJs at the expense of IH-

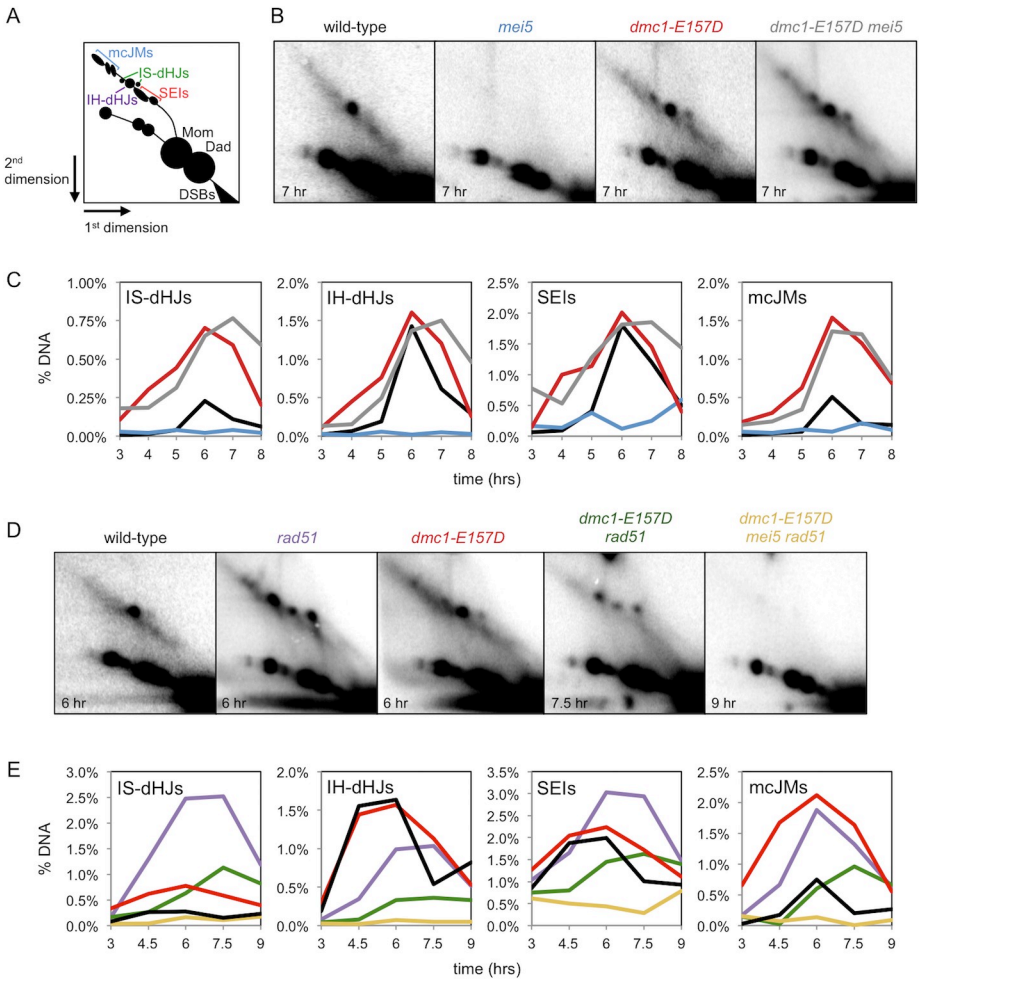

Fig 3. Recombination in *dmc1-E157D* is abnormal and dependent on Rad51, with little effect of Mei5-Sae3. (a) JMs that can be detected at the *HIS4*::*LEU2* meiotic recombination hotspot. (b) Southern analysis at the *HIS4*::*LEU2* hotspot from meiotic time course experiments following 2D gel electrophoresis. Time point for representative image is shown in the bottom left corner. (c) 2D gel quantitation; black–wild-type, light blue–*mei5*, red–*dmc1-E157D*, gray–*dmc1-E157D mei5*. (d) 2D gels as in (b). (e) 2D gel quantitation; black–wild-type, light purple–*rad51*, red–*dmc1-E157D*, green–*dmc1-E157D rad51*, yellow–*dmc1-E157D mei5 rad51*. Strains used in experiments in the order in which they appear in figure, left to right and top to bottom: DKB3698, DKB6320, DKB6342, DKB6300, DKB3710, DKB6393, DKB6412.

https://doi.org/10.1371/journal.pgen.1008217.g003

dHJs. The profound defect in IH bias in *dmc1-E157D rad51* contrasts with the *dmc1-E157D* single mutant, in which the IH-dHJ/IS-dHJ ratio is ~1.6. We conclude that *rad51* is epistatic to *dmc1-E157D* with respect to its impact on partner choice. The impact of a *rad51* mutation on the IH/IS ratio in *dmc1-E157D* cells further supports the view that the mechanism of IH bias is intact in *dmc1-E157D mei5* cells and therefore the conclusion that Mei5-Sae3 is not required for IH bias. The levels of IS-dHJs, IH-dHJs, SEIs, and mcJMs are all reduced approximately 2-fold in *dmc1-E157D rad51* relative to *rad51* (Fig 3E); thus, the hyper-recombinant phenotype of *dmc1-E157D* cells is Rad51-dependent. These findings are also consistent with the observation that CO levels in *dmc1-E157D* are reduced about 2-fold by the *rad51* mutation (Fig 2B).

JM formation is absent in triple mutant *dmc1-E157D mei5 rad51*

We also analyzed the *dmc1-E157D mei5 rad51* triple mutant by 2D gel electrophoresis. Surprisingly, while both *dmc1-E157D mei5* and *dmc1-E157D rad51* formed readily-detectable levels of JMs (Fig 3B and 3D), and Dmc1 foci were detected in *dmc1-E157D mei5 rad51* spread meiotic nuclei (Fig 1C and 1D), no JMs were detected in the triple mutant (Fig 3D and 3E). Because *rad51* strains are genetically unstable, we constructed an independent *dmc1-E157D mei5 rad51* diploid and repeated this experiment to ensure that our original strain had not picked up an additional mutation that suppressed the formation of JMs. Meiotic JMs were also undetectable in the duplicate *dmc1-E157D mei5 rad51* strain (S5 Fig). Given that resected and unrepaired DSBs trigger delays in meiotic progression, the 2D gel analyses are consistent with our finding that only ~10% of cells progress through a meiotic division in *dmc1-E157D mei5 rad51*, and that there is hyper-resection and limited CO formation in this strain (Fig 2A and 2B). We conclude that recombination is further compromised in the triple mutant *dmc1-E157D mei5 rad51* when compared to either double mutant. These results provide additional evidence that although Dmc1-E157D's activity is essentially Mei5-Sae3 independent in *RAD51*$^+$ cells, Mei5-Sae3 can promote limited Dmc1-E157D activity when Rad51 is absent.

The defects associated with *dmc1-E157D* and *dmc1-E157D mei5* are independent of Rad51's catalytic activity

One possible explanation for the results we obtained from our JM analysis in Fig 3 is that the *dmc1-E157D* mutation changes the behavior of Dmc1 in a manner that activates the strand exchange activity of Rad51. This possibility is emphasized by previous results suggesting that Dmc1 itself inhibits Rad51's strand exchange activity [87,88]. Normally, Rad51's strand exchange activity is repressed by Dmc1 and by the meiosis-specific Rad51 inhibitor Hed1 [3,76]. However, it was important to determine if Rad51's strand exchange activity plays a greater role in promoting recombination in *dmc1-E157D* cells than in wild-type [88]. To test this, we crossed the *rad51-II3A* mutation into our *dmc1-E157D* strains. The three alanine substitutions coded by *rad51-II3A* eliminate DNA binding site II, the secondary, low affinity DNA binding site required for homology searching. Rad51-II3A forms filaments, but lacks the ability to catalyze D-loop formation [3].

Our results indicate that the *rad51-II3A* mutation does not alter the efficiency and pattern of JM formation in the *dmc1-E157D* mutant (S6 Fig). This observation indicates that Dmc1, not Rad51, promotes the majority of homology search and strand exchange in *dmc1-E157D* cells, as is the case in wild-type cells. Thus, the hyper-recombinant phenotype observed in *dmc1-E157D* results from increased Dmc1 activity rather than activation of Rad51's activity. On the other hand, *rad51-II3A* causes a greater reduction in spore viability in a *dmc1-E157D* background than in a wild-type background (Table 1; from 57.6% to 17.0% for *dmc1-E157D* compared to 98.6% to 82.9% for *DMC1*$^+$, $p < 0.01$). The modest reduction in viability seen in *rad51-II3A* single mutants was previously interpreted to suggest that Rad51's strand exchange activity is only required at a small subset of the roughly 200 DSB sites where Dmc1-dependent DSB repair fails [3]. In the context of this interpretation, the data presented here can be explained if the fraction of attempted recombination events that require Rad51's strand exchange activity, although still small, is higher in *dmc1-E157D* than in wild-type.

Meiotic two-hybrid analysis indicates that direct Rad51-Dmc1 interaction is independent of Mei5

The results presented in Fig 3 show that Rad51 can impact Dmc1's activity in the absence of Mei5-Sae3. To determine if Rad51's influence on Dmc1 can be explained by direct interaction

of the two proteins, we carried out meiotic two-hybrid analysis. A previous two-hybrid study in budding yeast using the conventional mitotic method detected a low level of direct interaction between Rad51 and Dmc1, although the authors of that study did not ascribe significance to the interaction because it was much weaker than that observed for homotypic Rad51-Rad51 and Dmc1-Dmc1 interactions [89]. We wished to determine if Mei5-Sae3 enhanced the interaction between the two proteins and therefore used the meiotic two-hybrid method to test the interaction in a cell type that expresses the accessory protein. As in the previous study, the level of interaction observed for Rad51-Dmc1 was much lower than that in the Rad51-Rad51 and Dmc1-Dmc1 homotypic controls, but nonetheless reproducibly higher than the background level observed in empty vector controls (S7 Fig). Importantly, an equivalent two-hybrid signal was detected in a *mei5* background as in a wild-type background ($p = 0.5$ using a Wilcoxon signed-rank test) indicating that, in this system, Rad51-Dmc1 interaction is independent of Mei5-Sae3.

Super-resolution imaging of *dmc1-E157D* mutants reveals abnormalities in Dmc1 and RPA foci

Because Dmc1-E157D forms foci at high density, we expected that the wide-field microscopy method was not resolving closely spaced foci. Therefore, in order to obtain more accurate focus measurements, we re-examined chromosome spreads using stimulated emission depletion (STED) microscopy, which improves the resolution limit from around 200 nanometers (nm) to under 50 nm (see Methods Section, S8 Fig). For each strain, we imaged at least 13 randomly selected RPA-positive nuclei (Fig 4A). The average number of RPA foci detected was lowest in wild-type (70.0 ± 22.2 foci) (Fig 4B). All other strains displayed higher average RPA focus counts including *rad51* (140.5 ± 44.9 foci), *dmc1-E157D* (111.5 ± 28.8 foci), *dmc1-E157D mei5* (130.8 ± 21.2 foci), *dmc1-E157D rad51* (132.0 ± 21.7 foci), and *dmc1-E157D mei5 rad51* (131.3 ± 38.6 foci). We also measured focus lengths, and found that wild-type RPA foci are the shortest (76.8 ± 27.0 nm), while *rad51*, *dmc1-E157D rad51*, and *dmc1-E157D mei5 rad51* foci are all significantly longer (134.0 ± 70.4 nm, 136.0 ± 77.8 nm, 130.8 ± 63.8 nm respectively; $p < 0.01$, Wilcoxon test), but not significantly different from one another (pairwise $p = 0.53$, 0.60, and 0.94, respectively) (Fig 4C). The fact that RPA foci are longer in these strains is unsurprising given that we observed hyper-resection in these strains by 1D gel electrophoresis (Fig 2A). *dmc1-E157D* and *dmc1-E157D mei5* mutant RPA foci are significantly different from both wild-type and *rad51* mutants (107.4 ± 49.5 nm, 97.7 ± 39.6 nm respectively; $p < 0.01$), being an intermediate average length between the two. This finding contrasts with our Southern blotting analysis of DSBs (Fig 2A and S2 Fig), in which little to no difference between these two mutants and wild-type was detected with respect to resection tract lengths (see Discussion).

The average number of Dmc1 foci per nucleus was similar in wild-type and *rad51* single mutants (26.9 ± 17.7 foci and 23.3 ± 12.8 foci, respectively, Fig 4A and 4B). All *dmc1-E157D* strains displayed higher than normal focus counts including *dmc1-E157D* (114.0 ± 21.0 foci), *dmc1-E157D mei5* (119.2 ± 25.6 foci), *dmc1-E157D rad51* (105.3 ± 27.0 foci), and *dmc1-E157D mei5 rad51* (106.8 ± 23.8 foci) (Fig 4B). This result can be explained by the mutant's ability to form DSB-independent foci, by a longer lifespan of DSB-dependent foci, and/or by an increase in the total number of DSBs formed (Fig 1E, S2 Fig). We also measured the lengths of these Dmc1 foci, and found that Dmc1 foci are significantly shorter in *rad51* (82.5 ± 30.0 nm, $p < 0.01$, Wilcoxon test) than wild-type (97.1 ± 38.8 nm) (Fig 4C), consistent with previous wide-field microscopy analyses [78]. Dmc1 foci are longer in all *dmc1-E157D* strains, including *dmc1-E157D* (134.1 ± 61.5 nm, $p < 0.01$), *dmc1-E157D mei5* (147.1 ± 66.4 nm, $p < 0.01$),

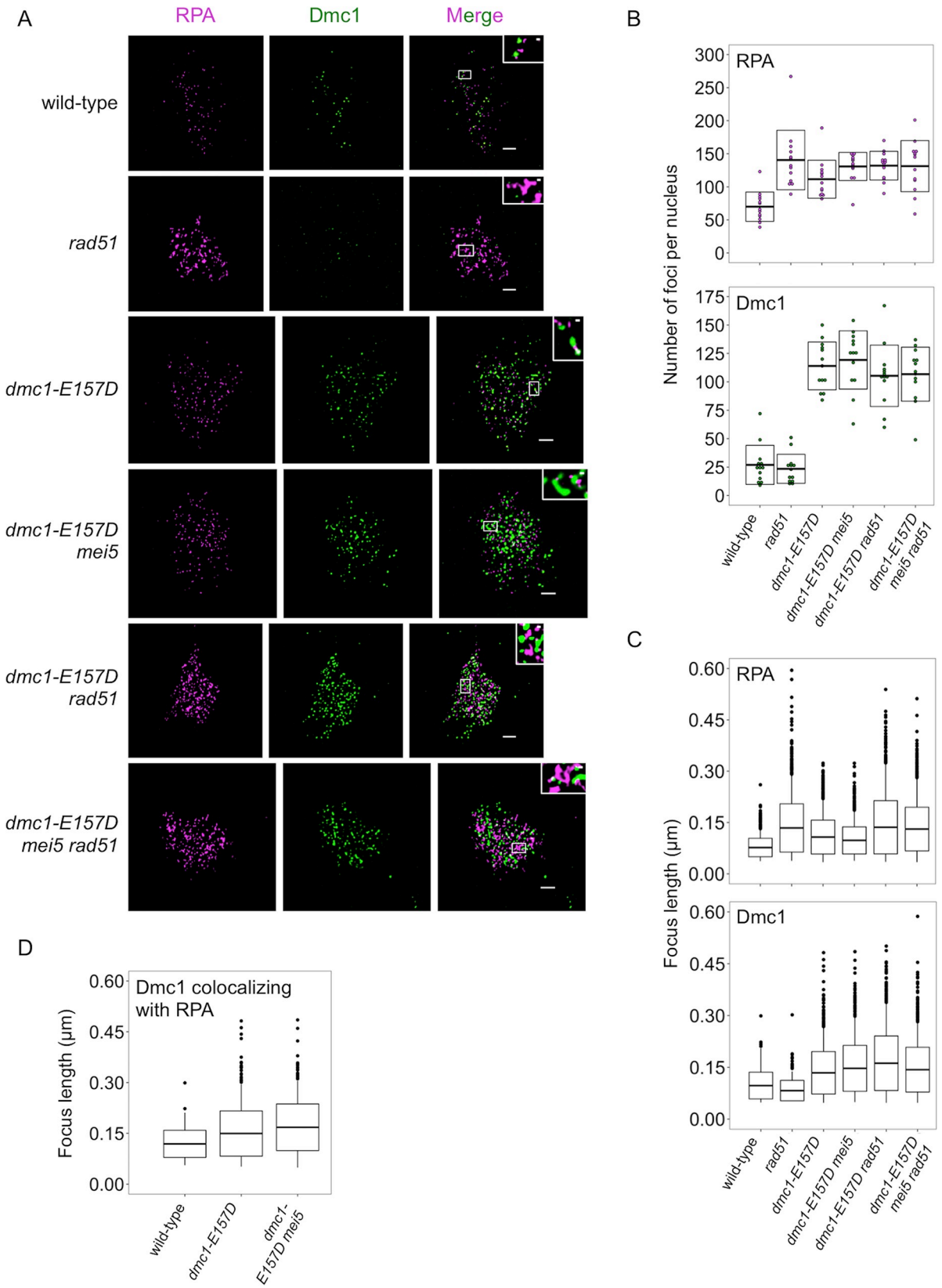
A
RPA
Dmc1
Merge
wild-type
rad51
dmc1-E157D
dmc1-E157D mei5
dmc1-E157D rad51
dmc1-E157D mei5 rad51
B
RPA
Dmc1
Number of foci per nucleus
wild-type
rad51
dmc1-E157D
dmc1-E157D mei5
dmc1-E157D rad51
dmc1-E157D mei5 rad51
C
RPA
Dmc1
Focus length (μm)
D
Dmc1 colocalizing with RPA
Focus length (μm)
wild-type
dmc1-E157D
dmc1-E157D mei5

Fig 4. Super-resolution imaging shows abnormalities in RPA, Dmc1 foci in mutants. (a) Representative STED microscopy imaging of spread meiotic nuclei are shown for each strain. Scale bars represent 1 μm; scale bars in inset represent 0.1 μm. For *dmc1-E157D mei5*, time point was taken at 5 hours in sporulation media; for all other strains, time point was taken at 4.5 hours. (b) Quantitation of foci counts for Dmc1, RPA, is shown for each strain. For each strain, 13 randomly selected nuclei were quantitated. (c) Quantitation of RPA and Dmc1 foci lengths is shown for each strain. (d) Quantitation of Dmc1 foci lengths colocalizing with RPA is shown for the strains indicated. Strains used in this experiment in the order in which they appear in figure, top to bottom: DKB3698, DKB3710, DKB6342, DKB6300, DKB6393, DKB6412.

https://doi.org/10.1371/journal.pgen.1008217.g004

dmc1-E157D rad51 (161.9 ± 78.9 nm, $p < 0.01$), and *dmc1-E157D mei5 rad51* (143.3 ± 64.7 nm, $p < 0.01$) relative to wild-type (Fig 4C).

Although measurements of Dmc1 focus lengths shows that Dmc1-E157D makes longer than normal filaments overall, the fact that the protein likely forms high levels of off-pathway foci in addition to forming foci at sites of recombination raises the possibility that the long filaments observed might only be off-pathway forms, with no appreciable change in the average length of recombinogenic filaments. Furthermore, the fraction of recombinogenic foci could differ in different strains. For example, off-pathway Dmc1 foci may make up a larger fraction of the total Dmc1 foci in *dmc1-E157D* strains than in wild-type and *rad51*. To provide evidence that recombinogenic foci are longer on average, we examined the lengths of Dmc1 foci that colocalized with RPA. Given that all of the mutants have more RPA foci and some have more Dmc1 foci (Fig 4B), the level of fortuitous colocalization is expected to be higher in the mutants than in wild-type. We therefore estimated the frequency of fortuitous colocalization in all strains by a previously described method [83]. This method may yield an overestimate of fortuitous colocalization because the most focus dense region of each nucleus was used in the analysis. Only nuclei in which the level of observed colocalization exceeded the estimated fortuitous colocalization in the same image by more than 5% were considered informative for analysis. A total of 10/13 wild-type nuclei (35.5% experimental and 18.8% fortuitous), 10/13 *dmc1-E157D* nuclei (70.1% experimental and 58.6% fortuitous colocalization), and 6/13 *dmc1-E157D mei5* nuclei (69.1% experimental and 57.1% fortuitous colocalization) met our criterion for analysis, indicating that RPA-colocalization provides a meaningful criterion to identify a subset of Dmc1 foci enriched for recombinogenic as opposed to off-pathway structures in these cells. Because of higher focus density and average focus size, none of the *dmc1-E157D rad51* and *dmc1-E157D mei5 rad51* nuclei met our criterion for detection of true co-localization. The average contour length of Dmc1 filaments that colocalized with RPA was 118.9 ± 40.0 nm in wild-type, or ~100 nucleotides, similar to the corresponding value obtained using direct stochastic optical reconstruction microscopy (dSTORM), a different super-resolution light microscopy method (Fig 4D) [36]. The average focus length for RPA colocalizing Dmc1 foci in *dmc1-E157D* was significantly longer than wild-type (149.5 ± 66.8 nm, or ~ 160 nucleotides, $p<0.01$, Wilcoxon test), and also different from the total population of unselected Dmc1 foci in *dmc1-E157D* cells (134.1 ± 61.5 nm). The average focus length for RPA colocalizing Dmc1 foci in *dmc1-E157D mei5* was also significantly longer than in wild-type (168.0 ± 66.4 nm, or ~190 nucleotides, $p <0.01$), and different from the total Dmc1 foci lengths in that background (147.1 ± 66.4 nm). Thus, Dmc1-E157D not only makes longer foci overall, but Dmc1-E157D foci associated with RPA-marked recombination sites are also distinctly longer under conditions of hyper-recombination (i.e. in *dmc1-E157D* and *dmc1-E157D mei5*) compared to wild-type.

Rhd54 promotes meiotic progression in *dmc1-E157D* cells

The cytological results presented above suggest that Dmc1-E157D is more likely than Dmc1-WT to form off-pathway filaments on dsDNA. DSB-independent foci are only easily

detected for Dmc1-WT when Rdh54, the key translocase involved in disassembling them, is absent [51]. This observation suggested that Dmc1-E157D might be more resistant to dsDNA dissociation by Rdh54. To determine whether Rdh54 was active in *dmc1-E157D* mutants, we constructed the *dmc1-E157D rdh54* double mutant. If Rdh54 is inefficient at promoting Dmc1-E157D dissociation from dsDNA, loss of Rdh54 in the *dmc1-E157D* background should be inconsequential. Instead, we find that although both *dmc1-E157D* and *rdh54* single mutants progress through meiosis to form tetrads in which roughly 50% or more of spores are viable, the *dmc1-E157D rdh54* double mutant arrested in prophase and failed to form spores (Table 1; S9 Fig). Thus, Rdh54 is active in *dmc1-E157D* cells.

Mei5-Sae3 is not required for the DSB-independent foci formed by Dmc1-WT protein in the absence of Rdh54

Dmc1-E157D differs from Dmc1-WT in that it forms high levels of off-pathway foci and does so independently of Mei5-Sae3. This suggests that although the mutant bypasses the requirement for Mei5-Sae3 with respect to forming recombinogenic foci, it might not fully recapitulate Mei5-Sae3 function because Mei5-Sae3's activity has only been shown to display DSB-dependent foci. It was not known if Mei5-Sae3 is also required for the off-pathway Dmc1 foci that accumulate when disassembly of dsDNA bound structures is blocked by *RDH54*$^{+}$ deletion. Therefore, to determine if Mei5-Sae3 is normally required for Dmc1 to form off-pathway complexes on dsDNA *in vivo*, we compared Dmc1 focus formation in *spo11 rdh54 mei5* to that in the *spo11 rdh54* double mutant; a *spo11* single mutant served as the negative control. The controls generated the expected results with *spo11 rdh54* nuclei displaying an average of 37 ± 14 Dmc1 foci per nucleus and *spo11* nuclei an average of only 3 ± 4 foci per nucleus (S10 Fig). The *spo11 rdh54 mei5* triple mutant displayed an average of 37 ± 13 foci, like the positive control, indicating that off-pathway focus formation by Dmc1-WT protein occurs independently of Mei5. Thus, Mei5-Sae3's function is dispensable for nucleation of Dmc1 complexes on dsDNA that are substrates for Rdh54-mediated disassembly. The implications of this finding are discussed below.

Discussion

The mechanism of Mei5-Sae3-mediated Dmc1 filament formation

Dmc1-E157D was designed to mimic the activity of the previously characterized bacterial protein RecA-E96D. Assuming this prediction is correct and Dmc1-E157D has reduced ATPase activity, our results provide *in vivo* support for the conclusion of Chi and colleagues that Sfr1-Swi5 acts to stabilize Rad51 filaments by promoting ADP release, thereby maintaining the filament in the active, ATP-bound form [69], given that a mutation designed to favor the ATP bound form of Dmc1 bypasses the normal requirement for Mei5-Sae3. On the other hand, the regulatory defects observed in Dmc1-E157D suggest that the function of Mei5-Sae3-mediated regulation may involve more than overall enhancement of Dmc1 filament stability, because the Dmc1-E157D mutant displays abnormally high levels of *spo11*-independent Dmc1-E157D binding to chromosomes (Fig 1E). We also find that although Mei5-Sae3 is required for cytologically detectable Dmc1 focus formation at sites of DSBs in wild-type cells, it is not required to observe the off-pathway dsDNA-bound foci formed by Dmc1-WT in *rdh54* cells (S10 Fig). These findings raise the possibility that stabilizing the ATP-bound form of Dmc1 alone may not fully explain Mei5-Sae3 function; it is possible that Mei5-Sae3 also confers ssDNA specificity to Dmc1-DNA interaction *in vivo*. The proposal that Mei5-Sae3 recruits Dmc1 to ssDNA is consistent with prior observations that Mei5-Sae3 preferentially binds ssDNA, and that it

directly interacts with the ssDNA-specific protein RPA [60,67,70]. Thus, Mei5-Sae3 may combine the ability to enhance Dmc1 filament stability with the ability to specifically promote filament formation on ssDNA rather than dsDNA. An alternative explanation, which we cannot rule out at present, is that Mei5-Sae3 enhances the affinity of Dmc1 for both ssDNA and dsDNA equally, but that the concentration of available dsDNA exceeds the K_D for Dmc1 binding in the absence of Mei5-Sae3, while the concentration of ssDNA does not. Further studies are required to determine if either the ssDNA or the RPA binding activities of Mei5-Sae3 recruit Dmc1 to ssDNA tracts.

The ability of Dmc1-E157D to form functional filaments on ssDNA *in vivo* in the absence of Mei5-Sae3, and to do so by a mechanism involving filament stabilization, raises the possibility that Dmc1 recruitment to and nucleation on RPA coated ssDNA in wild-type cells is not reliant on Mei5-Sae3. Given that Mei5-Sae3 binds directly to both Dmc1 and RPA [62,63,70], we continue to favor models in which Mei5-Sae3 plays a role in recruitment/nucleation of Dmc1 filaments. We note, however, that Dmc1 could be recruited to sites of DSBs through its interactions with RPA [60], and that nucleation, but not filament elongation, could be Mei5--Sae3 independent. Dmc1 nucleation events might be undetected in the absence of Mei5-Sae3 because the resulting filaments never elongate to lengths sufficient to reach the threshold of cytological detection. It is also possible that Rad51 is normally partially responsible for Dmc1 recruitment/nucleation, in addition to its roles in filament stabilization and IH bias. These considerations highlight the need for further studies on the mechanism of Dmc1 recruitment/nucleation on RPA coated ssDNA tracts *in vivo*.

The role of Rad51 in Dmc1 filament dynamics

The absence of foci observed in *mei5*, *sae3*, and *mei5 sae3* mutants, and the dimmer foci observed in *rad51* mutants, indicate that normal Dmc1 focus formation involves both proteins [61,62,78]. The fact that recombination and DSB-dependent focus formation in *rad51* yeast depends on Mei5-Sae3 suggests that Mei5-Sae3 is epistatic to Rad51. Furthermore, the formation of brightly staining Mei5-Sae3 foci depends on Rad51, as does the formation of brightly staining Dmc1 foci [62,78]. These dependency relationships raised the possibility that Rad51's ability to influence Dmc1 filaments might require a direct interaction between Rad51 and Mei5-Sae3 [90]. However, the data presented here indicate that Rad51 promotes formation of functional Dmc1 filaments on ssDNA independently of Mei5-Sae3, thus Rad51's normal influence on Dmc1 filament dynamics does not require, and may not involve, Mei5-Sae3 binding to Rad51.

Our data provide critical evidence that Mei5-Sae3 and Rad51 function independently with respect to enhancing the formation of functional Dmc1 filaments. Whereas *dmc1-E157D mei5* forms COs at a level nearly equivalent to wild-type, *dmc1-E157D rad51* suffers a dramatic reduction in CO formation, and experiences hyper-resection (Fig 2A and 2B). In addition, 2D gel electrophoresis shows that JM formation in *dmc1-E157D mei5* is equivalent to *dmc1-E157D*, while the JMs formed in the *dmc1-E157D rad51* background are significantly reduced relative to *dmc1-E157D*, and show an IH bias defect like the *rad51* single mutant (Fig 3D and 3E). Thus, a mutation that alleviates Dmc1's need for Mei5-Sae3, retains full dependency on Rad51. If the functions of Mei5-Sae3 and Rad51 were interdependent, a mutation that bypasses the requirement for Mei5-Sae3 would also bypass the requirement for Rad51. Under this model for independent function of the two accessory proteins, the partial dependency of Mei5-Sae3 foci on Rad51 can be explained if Mei5-Sae3 binds Dmc1 filaments along their entire contour, because Dmc1 forms shorter filaments in the absence of Rad51.

Rad51 is likely to impact Dmc1 filament dynamics by direct interaction. Although a previous study did not ascribe significance to the low level of interaction detected between budding

yeast Rad51 and Dmc1 [89], two-hybrid studies in other organisms detected significant levels of Rad51-Dmc1 interaction, albeit at low levels compared to the homotypic interactions [91–93]. Budding yeast Rad51 binds Dmc1 directly when pure proteins are mixed [60], consistent with similar observations in other organisms [91–93]. Using the meiotic two-hybrid method, we were able to detect Rad51-Dmc1 interaction during meiotic prophase of budding yeast, and to show that this interaction does not require Mei5-Sae3 (S7 Fig). These findings provide additional evidence that Rad51 and Mei5-Sae3 influence Dmc1 DNA binding dynamics independently. The finding that Rad51-Dmc1 interaction occurs, but is weaker than homotypic interactions, is consistent with a single molecule study that showed mixtures of Rad51 and Dmc1 form predominantly homo-filaments on DNA [31], and with prior cytological studies that showed the foci formed by Rad51 and Dmc1 lie adjacent to one another rather than being perfectly colocalized [61,89,94]. Finally, we note that direct interaction between the two proteins can account for the observation that Rad51 can stimulate Dmc1-mediated D-loop formation in the absence of other proteins [3].

How might Mei5-Sae3 and Rad51 promote Dmc1 filament stability by independent mechanisms? There are at least two basic mechanisms that could contribute to filament stability. First, an accessory protein could promote the high-affinity ssDNA binding form. Second, if a strand exchange protein is normally subject to enzymatically-driven disassembly, an accessory protein might act by specifically blocking the activity of that enzyme. Mei5-Sae3's role in filament stabilization *in vivo* almost certainly involves direct enhancement of DNA binding activity during nucleation and/or elongation, as is the case for Mei5-Sae3 homolog Sfr1-Swi5 [72]. Rad51 might also enhance binding directly, by reducing the off-rate of protomers from filaments. For example, a Rad51 monomer bound to the end of a Dmc1 filament might drastically reduce the off-rate of the adjacent Dmc1 protomer with a strong overall effect on filament stability, given that disassembly of filaments is expected to occur from filament ends [95].

Alternatively, or in addition, Rad51 may block a mechanism that actively dissociates Dmc1 filaments. Although no active disassembly mechanism has been identified for Dmc1 filaments, active disassembly could involve a helicase mechanism, similar to that mediated by UvrD and Srs2 [26–29]. One observation that appears to be at odds with the idea that Rad51 functions to promote Dmc1 filament formation by blocking an Srs2-like mechanism is that Rad51 stimulates Dmc1's D-loop activity in a purified system that does not include an ssDNA-specific helicase. However, it is possible that the *in vitro* activity of Rad51 in stimulating Dmc1 does not fully recapitulate the *in vivo* function of the protein. This possibility is emphasized by previous work on the Rad51 accessory factor Rad55-Rad57. Both subunits of the Rad55-Rad57 heterodimer are structurally similar to Rad51. Rad55-Rad57 stimulates Rad51 activity *in vitro*, but *in vivo* it additionally functions to limit the Rad51 strippase activity of Srs2 [96,97]. Thus, Rad51's impact on Dmc1 activity *in vitro* might similarly not fully represent its *in vivo* role in promoting stable Dmc1 filaments.

A model invoking inhibition of Dmc1-ssDNA filament disassembly can account for the fact that *dmc1-E157D rad51* forms fewer JMs relative to *DMC1*$^{+}$ *rad51* (Fig 3E). Like Dmc1-E157D, the Rad51 ATPase mutant Rad51-K191R is defective in recruitment to DSB-associated tracts of ssDNA *in vivo*. The DNA binding defect of Rad51-K191R is partially suppressed by deletion of *SRS2* or by overexpression of *RAD54* [55,56]. These findings suggest that the recruitment defect displayed by Rad51-K191R results from a combination of the protein's DNA binding defect, increased off-pathway dsDNA binding, and active disassembly of Rad51-K191R filaments that do form at DSB-associated tracts of ssDNA [57]. If Dmc1-E157D filaments form more slowly than wild-type filaments as a result of increased off-pathway binding, which would result in a decreased pool of free Dmc1 protomers, Dmc1-E157D filaments may be acutely sensitive to disassembly and/or end dissociation, thus explaining

Dmc1-E157D's dependency on Rad51. In addition, these models can account for the more severe phenotype of the *dmc1-E157D mei5 rad51* triple mutant compared to the *dmc1-E157D rad51* double mutant as a consequence of Mei5-Sae3 having a limited ability to block dissociation, or being able to promote fast reassembly. Such an activity of Mei5-Sae3 might be inconsequential for Dmc1-E157D DNA binding dynamics *in vivo* when Rad51 is present, explaining why the phenotypes of *dmc1-E157D* and *dmc1-E157D mei5* are nearly identical.

Mei5-Sae3 is not required for IH bias

The results presented here also reveal for the first time that although both Rad51 and Mei5-Sae3 promote the formation of stable Dmc1 filaments, Mei5-Sae3 differs from Rad51 in that Mei5-Sae3 is not required for IH bias while Rad51 is. This conclusion could not have been arrived at based on earlier observations because recombination is blocked prior to formation of JMs in *DMC1*$^+$ *mei5* and *DMC1*$^+$ *sae3* cells; bypass of the requirement for Mei5-Sae3 for formation of functional filaments allowed us to assess the role of Mei5-Sae3 in recombination partner choice at the strand invasion stage. Previous work showed that Rad51 and Dmc1 are both required for IH bias [79,88]. The results here show that the cooperation between Rad51 and Dmc1 required for IH bias involves a Rad51-dependent mechanism that is independent of Mei5-Sae3. This interpretation is consistent with the fact that, in other species, homologs of Mei5-Sae3 regulate Rad51 activity, suggesting that the Mei5-Sae3 family of accessory proteins solves a problem common to both Rad51 and Dmc1 that is not unique to meiotic recombination.

Chromatin immunoprecipitation experiments have shown that cells lacking both Rdh54 and Rad54 fail to recruit Dmc1 to DSB hotspots as a consequence of sequestration caused by off-pathway DNA binding. The failure to recruit Dmc1 to tracts of ssDNA accounts for the hyper-resection seen in *rad54 rdh54* double mutants [51,98]. Given that Dmc1-E157D forms foci in the absence of DSBs, and that it is modeled on RecA-E96D, which displays a lower than normal off-rate for dsDNA binding, one might expect that Dmc1-E157D is less efficiently removed from dsDNA by Rdh54 (and Rad54). Surprisingly, we find no evidence for a decrease in CO formation or for hyper-resection in *dmc1-E157D* (Fig 2A and 2B, S2 Fig). Moreover, dHJ formation is increased, suggesting that Dmc1-E157D is efficiently removed from the 3' end of the heteroduplex DNA to allow for recombination-associated DNA synthesis (Fig 3C and 3E). This function is likely carried out by Rdh54 given the corresponding activity of Rad54 on Rad51 and on the evidence that Rdh54 acts to remove off-pathway Dmc1 complexes from dsDNA [49,51]. We also find that the meiotic progression and spore formation observed in *dmc1-E157D* mutants is strongly dependent on Rdh54, indicating that Rdh54 is active in *dmc1-E157D* mutants (Table 1, S9 Fig). Thus, although Dmc1-E157D likely forms more off-pathway foci than Dmc1-WT, Rdh54 is apparently able to have some effect on Dmc1-E157D, which we presume involves dissociating the mutant Dmc1 protein from tracts of dsDNA.

Dmc1-E157D forms abnormally long filaments and is hyper-recombinant for certain JMs and recombination products

Although levels of IH CO intermediates and products are similar to those in wild-type, *dmc1-E157D* and *dmc1-E157D mei5* display higher than normal levels of certain types of recombination intermediates and products including IS-dHJs, mcJMs, and ectopic COs. For simplicity, we will refer to these unusual types of recombination events collectively as "aberrant," but we emphasize that all three types are observed at low levels in wild-type cells. IS-dHJs, mcJMs, and ectopic COs are all elevated about 3-fold in *dmc1-E157D* and *dmc1-E157D mei5* cells (Figs 2B, 3C and 3E, S4 Fig). The combination of aberrant recombination

phenotypes observed in *dmc1-E157D* cells is reminiscent of that reported for *sgs1*, *top3*, and *rmi1* mutants during meiosis [99–101]. Sgs1, Top3, and Rmi1 have been shown to form a complex, STR, that disassembles D-loops [102–104]. In addition, during mitotic recombination, STR was shown to have a role in disassembling aberrant invasion events in which a single Rad51 filament invades two or more donor molecules ("multi-invasions") [105]. This role of STR in multi-invasion disassembly was proposed to account for at least some of the phenotypes observed in the absence of Sgs1, Top3, or Rmi1 during meiosis [101]. In this context, maturation of a multi-invasion into a mcJM, followed by resolution of the multi-invasion, can account for the increase in mcJMs, IS-dHJs, and ectopic recombination observed in these mutants [106]. Further evidence that multi-invasions account for the meiotic STR mutant phenotypes is the fact that both multi-invasions and JMs in the *sgs1*, *top3*, or *rmi1* mutant backgrounds are highly dependent on structure-selective nucleases Mus81-Mms4, Slx1-Slx4, and Yen1 [100,101,105,107–109].

Several possibilities account for why *dmc1-E157D* and *dmc1-E157D mei5* are phenotypically similar to the *sgs1*, *top3*, and *rmi1* mutants. Dmc1-E157D may form the same number of aberrant intermediates as wild-type, but STR-mediated disassembly could be rendered less efficient as a consequence of enhanced binding activity of Dmc1-E157D compared to Dmc1-WT. Alternatively, as a consequence of the fact that Dmc1-E157D forms longer filaments, it may also form longer D-loops. Piazza et al. have recently shown that two D-loop disassembly pathways function in somatic cells, one that relies on the activities of STR and Mph1, and another that relies on Srs2 [104]. Interestingly, Srs2-dependent D-loops may be longer than those processed by the STR and Mph1 pathway [104,110]. Thus, if Dmc1-E157D forms longer D-loops, it may perturb the balance between these two D-loop editing pathways, resulting in the phenotypes observed. Arguing against the notion that D-loop disassembly is impaired by the *dmc1-E157D* mutation is the fact that there is no appreciable increase in SEIs in *dmc1-E157D* and *dmc1-E157D mei5* cells as compared to wild-type (Fig 3B and 3D), which might be expected if the mutant protein prevented D-loop disruption.

Our preferred model to account for the defects associated with *dmc1-E157D* and *dmc1-E157D mei5* is that Dmc1-E157D makes more aberrant D-loops than Dmc1-WT. In this model, STR, and possibly other helicases, disassemble aberrant D-loops normally, but the mutant protein generates more multi-invasions than Dmc1-WT. The two regions of homology engaged in such multi-invasion events could be on one sister and one homolog, or on both of the homologs, likely engaging one template at the allelic site, and one at the ectopic site. The formation of the multi-invasions can account for the increased mcJMs, while processing of multi-invasions to yield fully repaired chromatids can explain the increases in IS-dHJs and ectopic COs [106]. Drawing on the "intersegmental contact sampling" model of homology search [111], we propose Dmc1-E157D makes more multi-invasions as a consequence of making longer filaments (Fig 5). The intersegmental contact sampling model maintains that a filament has a polyvalent interaction surface capable of simultaneously searching multiple, non-contiguous dsDNA regions for homology [111]. Longer filaments are able to search duplex DNA more efficiently, as a consequence of being able to engage in a greater number of simultaneous interactions. We have demonstrated that Dmc1-E157D forms longer filaments *in vivo* (Fig 4C and 4D). We posit that because filaments are longer, Dmc1-E157D engages in a higher number of simultaneous searching interactions that results in more frequent homology-dependent engagement of two different regions of homology by a single filament. Given that multi-invasion recombination is thought to generate secondary DSBs [105,106], this interpretation explains not only the defects that we see by 2D gel electrophoresis (Fig 3B–3E) but also why DSBs accumulate to higher levels in *dmc1-E157D* relative to wild-type (S2 Fig) and persist longer (Fig 2A and 2B).

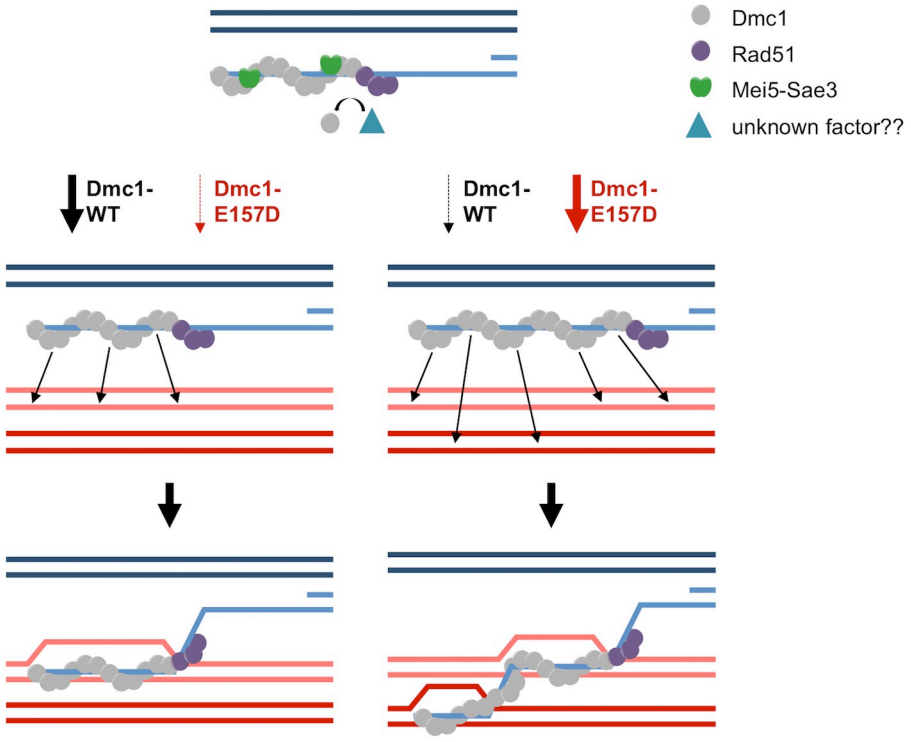

Fig 5. Model for regulation of filament length. Mei5-Sae3 and Rad51 promote Dmc1 filament formation and stability *in vivo*. A yet unknown ssDNA strippase may counterbalance their activities to limit filament length (depicted), or Dmc1 filament lengths may be limited by some other mechanism. This leads to the formation of relatively short Dmc1-WT filaments (~100 nts), which tend to make single invasions. In contrast, Dmc1-E157D filaments are no longer dependent on Mei5-Sae3, and longer filaments are formed on average. These longer Dmc1-E157D filaments are more prone to engage in multi-invasion recombination.

https://doi.org/10.1371/journal.pgen.1008217.g005

Though these aberrant recombination events are increased in *dmc1-E157D*, they also make up a substantial fraction of the recombination events observed in wild-type cells [99,105]. Consistent with this finding, 14% of wild-type Dmc1 foci that colocalized with RPA were longer than 149 nm in length, the average length of Dmc1-E157D foci that colocalize with RPA in *dmc1-E157D* (Fig 4D). This finding suggests that although most foci are much shorter than 149 nm in wild-type cells, long filaments do occasionally form. The proposal that longer than normal filaments are responsible for higher than normal levels of multi-invasions is supported by previous work showed that (1) if longer ssDNA substrates are used, there is a higher incidence of multi-invasions [112]; (2) Rad55-Rad57 promotes both longer Rad51 filaments and the formation of multi-invasions [97,106]; and (3) multi-invasions increased more than linearly as a consequence of increasing homology between the broken molecule and one of the two donors sequences [105].

The aberrant event hyper-recombinant phenotype displayed by Dmc1-E157D is Rad51-dependent. The mechanism responsible for Rad51's role in promoting the aberrant hyper-recombinant activity of Dmc1-E157D remains to be determined. Analysis of RPA co-localized foci provided evidence that Dmc1-E157D forms longer filaments on ssDNA in otherwise wild-type cells and in *mei5* single mutants. The mutant protein also forms long filaments on dsDNA, given that long filaments are also observed in *spo11* mutants (S8 Fig). Because both RPA and Dmc1 focus counts are increased in *dmc1-E157D rad51* and *dmc1-E157D mei5*

rad51 mutants (Fig 4B), and because both RPA and Dmc1 foci are also longer in these mutants (Fig 4C), it was not possible to identify a sub-population that we could be confident was enriched for ssDNA bound structures in these mutants. As a result, it is unclear if the dependency of Dmc1-E157D's hyper-recombinant phenotype on Rad51 reflects a requirement for Rad51 in forming long Dmc1 filaments on ssDNA, or if Rad51 plays some other role in promoting the high level of aberrant recombination events observed in *dmc1-E157D* and *dmc1-E157D mei5*. It is clear, however, that Rad51's homology search and strand exchange activities are not required for the aberrant hyper-recombinant phenotype observed in *dmc1-E157D* cells because IS-dHJs and mcJMs are increased in *dmc1-E157D rad51-II3A* cells, in a manner that is nearly indistinguishable from the *dmc1-E157D* single mutant (S6 Fig).

We speculate that the lengths of RecA-family strand exchange filaments are limited by regulatory mechanisms that evolved to prevent homology-dependent translocations and other genome rearrangements. Limiting filament lengths may limit the ability of filaments to simultaneously engage more than one homologous target sequence. In this regard, it is relevant that the single molecule study that provided evidence for intersegmental transfer did not detect any homology-dependent target engagement with the shortest ssDNA substrate examined, which was 162 nucleotides in length [111]. However, *in vivo*, Dmc1 filaments are typically ~100 nucleotides in wild-type cells (Fig 4C) [36]. Thus, it is possible that the cost of multi-invasions to genome stability has constrained the length of strand exchange filaments such that intersegmental searching is restricted or prevented *in vivo*.

Materials and methods

Yeast strains

The yeast strains used in this study are listed in S1 Table. All yeast strains are isogenic derivatives of strain SK-1.

To construct the *dmc1* point mutants, DKB plasmid pNRB628 containing the *DMC1* open reading frame, a 701 base pair upstream homology arm, the *TEF1* promoter, the *natMX4* open reading frame, the *ADH1* terminator, and a 40 base pair downstream homology arm, was modified by Gibson assembly to include the desired point mutations. *dmc1*::*LEU2-URA3-KAN* haploid yeast (DKB129, DKB130) were transformed with a linear PCR fragment containing the homology arms, the mutated *dmc1* open reading frame, and the *natMX4* (for resistance to nourseothricin sulfate, or cloNAT) selectable marker. Yeast were outgrown in 5 milliliters liquid YPDA for 4.5 hours at 30˚C in a culture rotator, then plated on selective media and allowed to grow at 30˚C for 3 days. After 3 days, colonies were struck out on the selective media and on 5-fluoroorotic acid (5-FOA), which selects against $URA3^{+}$ yeast and therefore identifies clones that have lost the *dmc1*::*LEU2-URA3-KAN* allele. Those colonies that grew on the cloNAT media and did not grow on the 5-FOA plates were tested to confirm proper targeting by polymerase chain reaction, and then confirmed via sequencing.

Meiotic time courses

Yeast cultures were induced to undergo synchronous meiosis as described previously [61]. Appropriate samples were collected at time points indicated in figures.

Spore viability

Spore viability was determined by tetrad dissection as the percent of spores that germinate and form a colony on a YPDA plate relative to the number expected if all dissected spores had lived.

Preparation and staining of spread yeast nuclei

Surface-spreading and immunostaining of meiotic yeast chromosomes on glass slides was performed as described previously [113]. Primary antibodies were used at the following dilutions: purified anti-goat Dmc1 bleed #4 DKB antibody #192 (1:800), anti-rabbit Rad51 bleed #2 DKB antibody #159 (1:1000), anti-rabbit RFA2 (1:1000), and anti-rabbit Hop2 bleed #3 DKB antibody #143 (1:1000). Secondary antibodies were used at a dilution of 1:1000 and included: Alexa Fluor 488 chicken anti-goat (Invitrogen by ThermoFisher Scientific), Alexa Fluor 594 donkey anti-rabbit (Invitrogen by ThermoFisher Scientific), Alexa Fluor 594 donkey anti-goat (Invitrogen by ThermoFisher Scientific) and Alexa Fluor 488 donkey anti-rabbit (Invitrogen by ThermoFisher Scientific). Images were collected on a Zeiss Axiovision 4.6 wide-field fluorescence microscope at 100X magnification. The same imaging parameters were used for all samples.

Wide-field microscopy analysis

For each strain, 50 or more adjacent and randomly selected nuclei were imaged. A field of nuclei was chosen for analysis based on the DAPI staining pattern. Nuclei were scored as focus positive if there were 3 or more immunostaining foci in a given nucleus. Due to focus crowding in wide-field images, it was not possible to generate reliable focus counts using automated methods. Therefore, focus counts were determined by eye for the experiments reported in S8 Fig.

One-dimensional gel electrophoresis

One-dimensional gel electrophoresis at the *HIS4*::*LEU2* meiotic hotspot was performed as follows. 15 milliliter sporulation media samples were collected at time points indicated from meiotic cultures. Sodium azide was added to a final concentration of 0.1%. Cells were spun down at 3000 rpm in tabletop clinical centrifuges for 5 minutes, then the supernatant was removed and the pellet was frozen at -20˚C. DNA was then purified as described previously [114]. Approximately 2 micrograms DNA per sample was then digested with XhoI or PstI (as indicated in figure legend) restriction enzyme (New England BioLabs) and processed as described previously [114]. Samples were then run on a 0.6% (XhoI) or 0.7% (PstI) agarose gel at 2V/cm for 24 (XhoI) or 18 (PstI) hours, followed by Southern blotting as described previously [86].

Two-dimensional gel electrophoresis

Two-dimensional gel electrophoresis at the *HIS4*:*LEU2* meiotic hotspot was performed as previously described [3].

Meiotic two-hybrid analysis

Analysis of Rad51-Dmc1 interaction in meiotic cells was performed using the meiotic two-hybrid method [115]. DNA binding domain constructs were transformed into *MATa* haploid strains DKB6431 (*MEI5*$^{+}$) and DKB6429 (*mei5*) and activation domain constructs were transformed into *MATα* haploid strains DKB6430 (*MEI5*$^{+}$) and DKB6428 (*mei5*). Independent transformants were mated to generate the diploid strains used for meiotic two hybrid experiments. 5 ml cultures were grown for 72 hours in synthetic tryptophan leucine dropout media to maintain 2μ plasmids and then transferred to YPD medium at OD600 = 0.2, and then grown for two generations before being transferred to SPS medium overnight, after which sporulation was induced on SPM-1/5COM medium. Recipes for media are as described previously [61]. Samples were prepared for β-galactosidase assays after 6 hours and 18 hours. The

plasmids used for the two-hybrid studies were derived from pGAD-C1 [116] for activation domain fusions, and from pCA1 a gift from Scott Keeney [115] for DNA binding domain fusions. Note that this system uses *E. coli lexA* as DNA binding domain for hybrid constructs in combination with a *lex-op*::*lacZ* reporter construct [115]. Plasmid designations and the markers carried by the plasmids were as follows: Dmc1BD = pNRB729 *2*μ, *TRP1*, P_{DMC1}-*DMC1-lexA*, *ampR*, *ori; Dmc1AD = pNRB271 2*μ, *LEU2*, P_{ADH}-*GAL4-AD*::*DMC1*, *ampR*, *ori*; Rad51BD = pNRB727 *2*μ, *TRP1*, P_{DMC1}-*lexA-Rad51*, *ampR*, *ori*; Rad51AD = pNRB688 *2*μ, *LEU2*, P_{ADH}-*GAL4-AD*::*RAD51*, *ampR*, *ori*; ΔBD = pNRB728 *2*μ, *TRP1*, P_{DMC1}-*lexA*, *ampR*, *ori*; and ΔAD = pNRB267 *2*μ, *LEU2*, P_{ADH}-*GAL4*, *ampR*, *ori*. Plasmid sequences are available on request.

Immunofluorescence imaging by STED microscopy

Spreads were stained using a protocol described previously [113] with the following modifications. Spreads were dipped in 0.2% Photo-Flo (Kodak) for 30 seconds, the excess was tapped off, and then the slides were washed in 1X TBS for 5 minutes. Spreads were then blocked with 300μL 3% BSA in 1X TBS. Following blocking, spreads were incubated with anti-goat Dmc1 (1:800) and anti-Rabbit RPA (1:1000) for $\geq$16 hours at 4˚C. Slides were then washed in 1X TBS + 0.05% Triton X-100 for 5 minutes with gentle rocking 7 times. Spreads were incubated with fluorochrome-conjugated secondary antibodies Alexa Fluor 594 donkey anti-goat and Alex Fluor 488 donkey anti-rabbit (1:1000) (ThermoFisher Scientific) for 2 hours at 4˚C, followed by washes as described. Slides were allowed to dry completely in fume hood, then 35μL Vectashield (Vector Laboratories, Inc.) was added, a coverslip was placed atop the slide, and the coverslip was sealed with nail polish.

Imaging was conducted on a Leica SP8 3D, 3-color Stimulated Emission Depletion (STED) Laser Scanning Confocal Microscope at the University of Chicago Integrated Light Microscopy Core Facility. The same imaging parameters were used for all strains. Images were deconvolved using Huygens software and applying the same settings for each image. Resolution is reported based on measurements taken from deconvolved images.

STED microscopy analysis

To quantitate the number of foci in each nucleus, the image channels were separated, and each channel image was converted to a binary image in ImageJ. The "Analyze Particles" function was used to obtain information regarding the number of foci in an image, the coordinates of the center of each focus, and the major length of each focus. The same settings were used to analyze all images. Colocalization between Dmc1 and RPA was scored in R using the coordinates given by ImageJ to calculate the distance between a given Dmc1 focus and all RPA foci in the nucleus. A Dmc1 focus was scored as colocalizing with a RPA focus if the nearest RPA focus was less than the length of that Dmc1 focus plus a preset RPA value that was calculated for each strain. The RPA value was calculated based on one half of the average length of all RPA foci in that sample plus one half of two standard deviations of that RPA length. This means that if a given Dmc1 focus is sitting side-by-side with an RPA focus, the distance between it and the center of the nearest RPA focus can be the length of that Dmc1 focus plus one half the average length of all RPA foci in that strain background, plus one half of two standard deviations of the RPA focus lengths. This calculation attempts to take into account the fact that both RPA foci and Dmc1 focus lengths vary from sample to sample. Plots and statistical tests were carried out in R using the ggplot and ggpubr packages.

Meiotic whole cell lysate, SDS-PAGE, and Western blotting

4 milliliters of meiotic culture was collected at the appropriate time point. Tricholoroacetic acid was added to a final concentration of 10% weight/volume. Samples were placed in a 60˚C water bath for 5 minutes, then placed on ice for 5 minutes. Next, samples were spun down at 3000 rotations per minute in a low-speed centrifuge, the supernatant removed by aspiration, and pellet then washed in ddH_2O. The pellet was then re-suspended in 1X-SDS-PAGE (60 mM TrisHCl pH 6.8, 0.05% SDS, 100 mM DTT, 5% glycerol) buffer supplemented with 50 mM sodium PIPES pH 7.5 to the appropriate concentration according to the optical density of cells in the sample. The samples were then boiled for 10 minutes, spun down, and pellets stored at -20˚C.

A 12% SDS-polyacrylamide gel was prepared, and 30 microliters of each sample was run at 120V for 1.5 hours alongside 20 nanograms purified Dmc1 protein. Samples were then transferred to Merck Millipore Limited Immobilon-P Transfer Membrane for 16 hours at 50V at 4˚C. The membrane was then blotted using anti-goat Dmc1 (1:1000) primary antibody and an anti-goat HRP-conjugated secondary antibody (1:1000).

Meiotic progression and MI segregation imaging

Differential interference contrast (DIC) and epifluorescence images were collected on an IX-81 microscope (Olympus, Tokyo, Japan) controlled by MetaMorph software (Molecular Devices, Sunnyvale, CA) and fitted with an Orca-ER camera (Hamamatsu, Bridgewater, NJ) and a 60X, 1.4 NA Plan Apo objective. Nuclear divisions were monitored by DAPI staining. Cells with two DAPI-staining bodies or a single DAPI-staining body that was stretched were scored as having initiated MI; cells with three or more DAPI bodies or an "X" shape were scored as undergoing meiosis II division.

Supporting information

S1 Fig. *DMC1* expression for wild-type, *dmc1-E157D*. Left column, W. blot against Dmc1 for 5μL sample prepared from meiotic yeast cultures at 6 hours as described in Methods Section for each strain. Control column is 20 ng purified Dmc1 protein that was run in parallel with sample and used to quantitate blots. Sample concentration is estimated concentration in comparison to 20 ng purified Dmc1 protein. Similar results were obtained from an independent meiotic time course. Strains used in this experiment in the order in which they appear in figure, top to bottom: DKB3698, DKB6342.
(PDF)

S2 Fig. Additional Southern blot analysis at the *HIS4*::*LEU2* hotspot. (a) Southern blot analysis at the *HIS4*::*LEU2* hotspot following digestion of genomic DNA from meiotic time course experiments with PstI. Time points and strains are indicated beneath each lane. Note that *dmc1-E157D rad51* is shown at late time points as a reference for hyper-resection. (b) Quantitation of 1D gels shown in (a); black–wild-type, red–*dmc1-E157D*. Strains used in experiments in the order in which they appear in figure, left to right: DKB3698, DKB6342, DKB6393.
(PDF)

S3 Fig. *spo11* suppresses the meiotic progression defect associated with *dmc1-E157D*. (a) Representative images showing MI segregation in the strains indicated. (b) Quantitation of MI division defects observed in the strains indicated. A "normal" division is defined as having two equally-sized and well-defined DAPI staining bodies, whereas an "abnormal" division is defined as having unequal DAPI bodies or DNA connecting the two DAPI bodies. (c) Meiotic progression data for strains indicated. For each time point, $\geq$50 cells were scored. Strains used

in this experiment in the order in which they appear in figure, top to bottom: DKB3698, DKB2123, DKB6342, DKB6419.
(PDF)

S4 Fig. JMs accumulate at the *HIS4*::*LEU2* recombination hotspot in the absence of *ndt80*. (a) Southern analysis at the *HIS4*::*LEU2* hotspot at 8 hours following 2D gel electrophoresis. (b) 2D gel quantitation; dark gray–*ndt80*, dark red–*ndt80 dmc1-E157D*. Quantitation for each strain represents an average of two independently cultured diploids. Strains used in this experiment in the order in which they appear in figure, left to right: DKB3689, DKB3428, DKB6676, DKB6682.
(PDF)

S5 Fig. Duplicate meiotic time course experiments for *dmc1-E157D rad51* and *dmc1-E157D mei5 rad51*. For *dmc1-E157D mei5 rad51*, two independently derived diploids were used. (a) Southern analysis at the *HIS4*::*LEU2* hotspot from meiotic time course experiments following 2D gel electrophoresis. Time point for representative image is shown in the bottom left corner. (b) 2D gel quantitation; black–wild-type, dark green–*dmc1-E157D rad51*, yellow–*dmc1-E157D mei5 rad51*. Strains used in this experiment in the order in which they appear in figure, left to right: DKB3698, DKB6393, DKB6413.
(PDF)

S6 Fig. The defects associated with *dmc1-E157D rad51* are independent of Rad51's catalytic activity. (a) Southern analysis at the *HIS4*::*LEU2* hotspot from meiotic time course experiments following 2D gel electrophoresis. Time point for representative image is shown in the bottom left corner. (b) 2D gel quantitation; gray–*rad51-II3A*, red–*dmc1-E157D*, dark blue–*dmc1-E157D rad51-II3A*. Strains used in this experiment in the order in which they appear in figure, right to left: DKB3689, DKB6342, DKB6400.
(PDF)

S7 Fig. Meiotic two-hybrid analysis detects a weak interaction between Rad51 and Dmc1 that is independent of Mei5. (a) All interactions examined are plotted. (b) Subset of the same data shown in (a) to facilitate comparison of measurements of the Rad51-Dmc1 interaction with empty vector controls. The difference between Dmc1AD+Rad51BD *mei5* and Dmc1AD +Rad51BD WT (wild-type) is not statistically significant ($p = 0.5$ using a Wilcoxon signed-rank test). ΔBD and ΔAD represent the empty vectors. Strains used in this experiment: DKB6501, DKB6503, DKB6508, DKB6509, DKB6513, DKB6515.
(PDF)

S8 Fig. Super-resolution imaging resolves closely spaced foci, but elongated Dmc1 foci still form in *spo11 dmc1-E157D*. (a) Spread meiotic nuclei prepared from a *dmc1-E157D mei5* 5 hour sample imaged using confocal and STED microscopy methods. (b) STED imaging of a *spo11 dmc1-E157D* spread meiotic nuclei at 5 hours. For both, scale bar represents 1 micrometer. Magenta, RPA, green, Dmc1. Strains used in this experiment: DKB6300, DKB6419.
(PDF)

S9 Fig. *dmc1-E157D rdh54* is more defective in meiotic progression than either of the single mutants, *dmc1-E157D* and *rdh54*. Meiotic progression data for strains indicated. For each time point, $\geq$100 cells were scored. Strains used in this experiment in the order in which they appear in figure, top to bottom: DKB2526, DKB6342, DKB6583.
(PDF)

S10 Fig. DSB-independent Dmc1-WT focus formation does not require Mei5. Samples were collected 4 hours after induction of meiosis in liquid medium and immuno-stained for Dmc1 and Hop2. Because Hop2 staining is Spo11 independent and specific for meiotic prophase, random prophase nuclei were selected on the basis of being Hop2 positive and then imaged for Dmc1 staining. 50 nuclei were examined for each sample with 3 representative nuclei shown for each of the three strains examined. Images were generated by wide-field microscopy using the same camera settings for all strains. Strains used in this experiment in the order in which they appear in figure, top to bottom: DKB2524, DKB2523, and DKB6571.
(PDF)

S1 Table. Yeast strains used in this study.
(PDF)

S1 Data. Spreadsheets with numerical data used to generate all Figures.
(XLSX)

Acknowledgments

We thank Wolf-Dietrich Heyer and Neil Hunter for helpful discussions and suggestions. Thanks to Akira Shinohara for the gift of the anti-rabbit RFA2 antibody, and Scott Keeney for the gift of the meiotic two-hybrid strains. We are grateful to Vytas Bindokas and Christine Labno for assistance with STED microscopy. Melissa Castiglione constructed the strains and one of the plasmids used in the two-hybrid analysis.

Author Contributions

Conceptualization: Diedre Reitz, Douglas K. Bishop.

Formal analysis: Diedre Reitz, Douglas K. Bishop.

Investigation: Diedre Reitz, Jennifer Grubb, Douglas K. Bishop.

Methodology: Diedre Reitz, Douglas K. Bishop.

Project administration: Douglas K. Bishop.

Supervision: Douglas K. Bishop.

Validation: Diedre Reitz.

Visualization: Diedre Reitz.

Writing – original draft: Diedre Reitz.

Writing – review & editing: Jennifer Grubb, Douglas K. Bishop.

References

1. Hunter N. Meiotic recombination: The essence of heredity. Cold Spring Harb Perspect Biol. 2015 Oct 28; 7(12):a016618–35. https://doi.org/10.1101/cshperspect.a016618 PMID: 26511629
2. Bishop DK, Park D, Xu L, Kleckner N. *DMC1*: a meiosis-specific yeast homolog of E. coli *recA* required for recombination, synaptonemal complex formation, and cell cycle progression. Cell. 1992 May 1; 69 (3):439–56. https://doi.org/10.1016/0092-8674(92)90446-j PMID: 1581960
3. Cloud V, Chan Y-L, Grubb J, Budke B, Bishop DK. Rad51 is an accessory factor for Dmc1-mediated joint molecule formation during meiosis. Science. 2012 Sep 7; 337(6099):1222–5. https://doi.org/10.1126/science.1219379 PMID: 22955832
4. Shinohara A, Ogawa H, Ogawa T. Rad51 protein involved in repair and recombination in S. cerevisiae is a RecA-like protein. Cell. 1992 May 1; 69(3):457–70. https://doi.org/10.1016/0092-8674(92)90447-k PMID: 1581961

5. Sung P, Robberson DL. DNA strand exchange mediated by a RAD51-ssDNA nucleoprotein filament with polarity opposite to that of RecA. Cell. 1995 Aug 11; 82(3):453–61. https://doi.org/10.1016/0092-8674(95)90434-4 PMID: 7634335
6. Keeney S, Giroux CN, Kleckner N. Meiosis-specific DNA double-strand breaks are catalyzed by Spo11, a member of a widely conserved protein family. Cell. 1997 Feb 7; 88(3):375–84. https://doi.org/10.1016/s0092-8674(00)81876-0 PMID: 9039264
7. Symington LS. Mechanism and regulation of DNA end resection in eukaryotes. Crit Rev Biochem Mol Biol. 2016 Apr 20; 51(3):195–212. https://doi.org/10.3109/10409238.2016.1172552 PMID: 27098756
8. Bell JC, Kowalczykowski SC. RecA: Regulation and mechanism of a molecular search engine. Trends Biochem Sci. 2016 Jun; 41(6):491–507. https://doi.org/10.1016/j.tibs.2016.04.002 PMID: 27156117
9. Jinks-Robertson S, Petes TD. High-frequency meiotic gene conversion between repeated genes on nonhomologous chromosomes in yeast. Proc Natl Acad Sci U S A. 1985 May; 82(10):3350–4. https://doi.org/10.1073/pnas.82.10.3350 PMID: 3889906
10. Lichten M, Borts RH, Haber JE. Meiotic gene conversion and crossing over between dispersed homologous sequences occurs frequently in *Saccharomyces cerevisiae*. Genetics. 1987 Feb; 115(2):233–46. PMID: 3549449
11. Goldman AS, Lichten M. The efficiency of meiotic recombination between dispersed sequences in *Saccharomyces cerevisiae* depends upon their chromosomal location. Genetics. 1996 Sep; 144 (1):43–55. PMID: 8878672
12. Grushcow JM, Holzen TM, Park KJ, Weinert T, Lichten M, Bishop DK. *Saccharomyces cerevisiae* checkpoint genes *MEC1*, *RAD17* and *RAD24* are required for normal meiotic recombination partner choice. Genetics. 1999 Oct; 153(2):607–20. PMID: 10511543
13. Schwacha A, Kleckner N. Identification of joint molecules that form frequently between homologs but rarely between sister chromatids during yeast meiosis. Cell. 1994 Jan 14; 76(1):51–63. https://doi.org/10.1016/0092-8674(94)90172-4 PMID: 8287479
14. Brown MS, Bishop DK. DNA strand exchange and RecA homologs in meiosis. Cold Spring Harb Perspect Biol. 2015 Jan 5; 7(1):a016659–31.
15. Wright WD, Shah SS, Heyer W-D. Homologous recombination and the repair of DNA double-strand breaks. J Biol Chem. 2018 Jul 6; 293(27):10524–35. https://doi.org/10.1074/jbc.TM118.000372 PMID: 29599286
16. McVey M, Khodaverdian VY, Meyer D, Cerqueira PG, Heyer W-D. Eukaryotic DNA polymerases in homologous recombination. Annu Rev Genet. 2016 Nov 23; 50(1):393–421.
17. McMahill MS, Sham CW, Bishop DK. Synthesis-dependent strand annealing in meiosis. PLoS Biol. 2007 Nov 6; 5(11):e299. https://doi.org/10.1371/journal.pbio.0050299 PMID: 17988174
18. Merker JD, Dominska M, Petes TD. Patterns of heteroduplex formation associated with the initiation of meiotic recombination in the yeast. Genetics. 2003 Sep; 165(1):47–63. PMID: 14504217
19. Allers T, Lichten M. Differential timing and control of noncrossover and crossover recombination during meiosis. Cell. 2001 Jul 13; 106(1):47–57. https://doi.org/10.1016/s0092-8674(01)00416-0 PMID: 11461701
20. Hunter N, Kleckner N. The single-end invasion: an asymmetric intermediate at the double-strand break to double-Holliday junction transition of meiotic recombination. Cell. 2001 Jul 13; 106(1):59–70. https://doi.org/10.1016/s0092-8674(01)00430-5 PMID: 11461702
21. Schwacha A, Kleckner N. Identification of double Holliday junctions as intermediates in meiotic recombination. Cell. 1995 Dec 1; 83(5):783–91. https://doi.org/10.1016/0092-8674(95)90191-4 PMID: 8521495
22. Zakharyevich K, Tang S, Ma Y, Hunter N. Delineation of joint molecule resolution pathways in meiosis identifies a crossover-specific resolvase. Cell. 2012 Apr 13; 149(2):334–47. https://doi.org/10.1016/j.cell.2012.03.023 PMID: 22500800
23. Heyer W-D. Regulation of recombination and genomic maintenance. Cold Spring Harb Perspect Biol. 2015 Aug 3; 7(8):a016501. https://doi.org/10.1101/cshperspect.a016501 PMID: 26238353
24. Krejci L, Altmannova V, Spirek M, Zhao X. Homologous recombination and its regulation. Nucleic Acids Res. 2012 Jul; 40(13):5795–818. https://doi.org/10.1093/nar/gks270 PMID: 22467216
25. Kowalczykowski SC. An overview of the molecular mechanisms of recombinational DNA repair. Cold Spring Harb Perspect Biol. 2015 Nov 2; 7(11).
26. Krejci L, Van Komen S, Li Y, Villemain J, Reddy MS, Klein H, et al. DNA helicase Srs2 disrupts the Rad51 presynaptic filament. Nature. 2003 May 15; 423(6937):305–9. https://doi.org/10.1038/nature01577 PMID: 12748644

27. Veaute X, Jeusset J, Soustelle C, Kowalczykowski SC, Le Cam E, Fabre F. The Srs2 helicase prevents recombination by disrupting Rad51 nucleoprotein filaments. Nature. 2003 May 15; 423 (6937):309–12. https://doi.org/10.1038/nature01585 PMID: 12748645

28. Veaute X, Delmas S, Selva M, Jeusset J, Le Cam E, Matic I, et al. UvrD helicase, unlike Rep helicase, dismantles RecA nucleoprotein filaments in *Escherichia coli*. EMBO J. 2005 Jan 12; 24(1):180–9. https://doi.org/10.1038/sj.emboj.7600485 PMID: 15565170

29. Petrova V, Chen SH, Molzberger ET, Tomko E, Chitteni-Pattu S, Jia H, et al. Active displacement of RecA filaments by UvrD translocase activity. Nucleic Acids Res. 2015 Apr 30; 43(8):4133–49. https://doi.org/10.1093/nar/gkv186 PMID: 25824953

30. Sasanuma H, Furihata Y, Shinohara M, Shinohara A. Remodeling of the Rad51 DNA strand-exchange protein by the Srs2 helicase. Genetics. 2013 Aug; 194(4):859–72. https://doi.org/10.1534/genetics.113.150615 PMID: 23770697

31. Crickard JB, Kaniecki K, Kwon Y, Sung P, Greene EC. Meiosis-specific recombinase Dmc1 is a potent inhibitor of the Srs2 antirecombinase. Proc Natl Acad Sci U S A. 2018 Oct 23; 115(43):E10041–8. https://doi.org/10.1073/pnas.1810457115 PMID: 30301803

32. Bishop DK, Ear U, Bhattacharyya A, Calderone C, Beckett M, Weichselbaum RR, et al. Xrcc3 is required for assembly of Rad51 complexes *in vivo*. J Biol Chem. 1998 Aug 21; 273(34):21482–8. https://doi.org/10.1074/jbc.273.34.21482 PMID: 9705276

33. Gasior SL, Olivares H, Ear U, Hari DM, Weichselbaum R, Bishop DK. Assembly of RecA-like recombinases: distinct roles for mediator proteins in mitosis and meiosis. Proc Natl Acad Sci U S A. 2001 Jul 17; 98(15):8411–8. https://doi.org/10.1073/pnas.121046198 PMID: 11459983

34. Haaf T, Golub EI, Reddy G, Radding CM, Ward DC. Nuclear foci of mammalian Rad51 recombination protein in somatic cells after DNA damage and its localization in synaptonemal complexes. Proc Natl Acad Sci U S A. 1995 Mar 14; 92(6):2298–302. https://doi.org/10.1073/pnas.92.6.2298 PMID: 7892263

35. Gataulin DV, Carey JN, Li J, Shah P, Grubb JT, Bishop DK. The ATPase activity of *E. coli* RecA prevents accumulation of toxic complexes formed by erroneous binding to undamaged double stranded DNA. Nucleic Acids Res. 2018 Oct 12; 46(18):9510–23. https://doi.org/10.1093/nar/gky748 PMID: 30137528

36. Brown MS, Grubb J, Zhang A, Rust MJ, Bishop DK. Small Rad51 and Dmc1 complexes often co-occupy both ends of a meiotic DNA double strand break. PLoS Genet. 2015 Dec; 11(12):e1005653. https://doi.org/10.1371/journal.pgen.1005653 PMID: 26719980

37. Egelman EH, Stasiak A. Structure of helical RecA-DNA complexes. Complexes formed in the presence of ATP-gamma-S or ATP. J Mol Biol. 1986 Oct 20; 191(4):677–97. https://doi.org/10.1016/0022-2836(86)90453-5 PMID: 2949085

38. Zakharyevich K, Ma Y, Tang S, Hwang PY-H, Boiteux S, Hunter N. Temporally and biochemically distinct activities of Exo1 during meiosis: double-strand break resection and resolution of double Holliday junctions. Mol Cell. 2010 Dec 22; 40(6):1001–15. https://doi.org/10.1016/j.molcel.2010.11.032 PMID: 21172664

39. Menetski JP, Bear DG, Kowalczykowski SC. Stable DNA heteroduplex formation catalyzed by the *Escherichia coli* RecA protein in the absence of ATP hydrolysis. Proc Natl Acad Sci U S A. 1990 Jan; 87(1):21–5. https://doi.org/10.1073/pnas.87.1.21 PMID: 2404275

40. Rosselli W, Stasiak A. Energetics of RecA-mediated recombination reactions. Without ATP hydrolysis RecA can mediate polar strand exchange but is unable to recycle. J Mol Biol. 1990 Nov 20; 216 (2):335–52. https://doi.org/10.1016/S0022-2836(05)80325-0 PMID: 2147722

41. Sung P, Stratton SA. Yeast Rad51 recombinase mediates polar DNA strand exchange in the absence of ATP hydrolysis. J Biol Chem. 1996 Nov 8; 271(45):27983–6. https://doi.org/10.1074/jbc.271.45.27983 PMID: 8910403

42. Campbell MJ, Davis RW. Toxic mutations in the *recA* gene of *E. coli* prevent proper chromosome segregation. J Mol Biol. 1999 Feb 19; 286(2):417–35. https://doi.org/10.1006/jmbi.1998.2456 PMID: 9973561

43. Stasiak A, Egelman EH. Visualization of recombination intermediates. Kucherlapati R, Smith GR, editors. Genetic Recombination. 1988:265–307.

44. Sung P. Catalysis of ATP-dependent homologous DNA pairing and strand exchange by yeast RAD51 protein. Science. 1994 Aug 26; 265(5176):1241–3. https://doi.org/10.1126/science.8066464 PMID: 8066464

45. Zaitseva EM, Zaitsev EN, Kowalczykowski SC. The DNA binding properties of *Saccharomyces cerevisiae* Rad51 protein. J Biol Chem. 1999 Jan 29; 274(5):2907–15. https://doi.org/10.1074/jbc.274.5.2907 PMID: 9915828

46. Hong EL, Shinohara A, Bishop DK. *Saccharomyces cerevisiae* Dmc1 protein promotes renaturation of single-strand DNA (ssDNA) and assimilation of ssDNA into homologous super-coiled duplex DNA. J Biol Chem. 2001 Nov 9; 276(45):41906–12. https://doi.org/10.1074/jbc.M105563200 PMID: 11551925

47. Solinger JA, Kiianitsa K, Heyer W-D. Rad54, a Swi2/Snf2-like recombinational repair protein, disassembles Rad51:dsDNA filaments. Mol Cell. 2002 Nov; 10(5):1175–88. https://doi.org/10.1016/s1097-2765(02)00743-8 PMID: 12453424

48. Sheridan SD, Yu X, Roth R, Heuser JE, Sehorn MG, Sung P, et al. A comparative analysis of Dmc1 and Rad51 nucleoprotein filaments. Nucleic Acids Res. 2008 Jul; 36(12):4057–66. https://doi.org/10.1093/nar/gkn352 PMID: 18535008

49. Li X, Heyer W-D. RAD54 controls access to the invading 3'-OH end after RAD51-mediated DNA strand invasion in homologous recombination in *Saccharomyces cerevisiae*. Nucleic Acids Res. 2009 Feb; 37(2):638–46. https://doi.org/10.1093/nar/gkn980 PMID: 19074197

50. Chi P, Kwon Y, Seong C, Epshtein A, Lam I, Sung P, et al. Yeast recombination factor Rdh54 functionally interacts with the Rad51 recombinase and catalyzes Rad51 removal from DNA. J Biol Chem. 2006 Sep 8; 281(36):26268–79. https://doi.org/10.1074/jbc.M602983200 PMID: 16831867

51. Holzen TM, Shah PP, Olivares HA, Bishop DK. Tid1/Rdh54 promotes dissociation of Dmc1 from non-recombinogenic sites on meiotic chromatin. Genes Dev. 2006 Sep 15; 20(18):2593–604. https://doi.org/10.1101/gad.1447106 PMID: 16980587

52. Shah PP, Zheng X, Epshtein A, Carey JN, Bishop DK, Klein HL. Swi2/Snf2-related translocases prevent accumulation of toxic Rad51 complexes during mitotic growth. Mol Cell. 2010 Sep 24; 39(6):862–72. https://doi.org/10.1016/j.molcel.2010.08.028 PMID: 20864034

53. Mason JM, Dusad K, Wright WD, Grubb J, Budke B, Heyer W-D, et al. RAD54 family translocases counter genotoxic effects of RAD51 in human tumor cells. Nucleic Acids Res. 2015 Mar 31; 43(6):3180–96. https://doi.org/10.1093/nar/gkv175 PMID: 25765654

54. Hilario J, Amitani I, Baskin RJ, Kowalczykowski SC. Direct imaging of human Rad51 nucleoprotein dynamics on individual DNA molecules. Proc Natl Acad Sci U S A. 2009 Jan 13; 106(2):361–8. https://doi.org/10.1073/pnas.0811965106 PMID: 19122145

55. Morgan EA, Shah N, Symington LS. The requirement for ATP hydrolysis by *Saccharomyces cerevisiae* Rad51 is bypassed by mating-type heterozygosity or *RAD54* in high copy. Mol Cell Biol. 2002 Sep; 22(18):6336–43. https://doi.org/10.1128/MCB.22.18.6336-6343.2002 PMID: 12192033

56. Fung CW, Fortin GS, Peterson SE, Symington LS. The *rad51-K191R* ATPase-defective mutant is impaired for presynaptic filament formation. Mol Cell Biol. 2006 Dec; 26(24):9544–54. https://doi.org/10.1128/MCB.00599-06 PMID: 17030607

57. Li X, Zhang X-P, Solinger JA, Kiianitsa K, Yu X, Egelman EH, et al. Rad51 and Rad54 ATPase activities are both required to modulate Rad51-dsDNA filament dynamics. Nucleic Acids Res. 2007; 35(12):4124–40. https://doi.org/10.1093/nar/gkm412 PMID: 17567608

58. Conway AB, Lynch TW, Zhang Y, Fortin GS, Fung CW, Symington LS, et al. Crystal structure of a Rad51 filament. Nat Struct Mol Biol. 2004 Aug; 11(8):791–6. https://doi.org/10.1038/nsmb795 PMID: 15235592

59. Galkin VE, Wu Y, Zhang X-P, Qian X, He Y, Yu X, et al. The Rad51/RadA N-terminal domain activates nucleoprotein filament ATPase activity. Structure. 2006 Jun; 14(6):983–92. https://doi.org/10.1016/j.str.2006.04.001 PMID: 16765891

60. Chan Y-L, Zhang A, Weissman BP, Bishop DK. RPA resolves conflicting activities of accessory proteins during reconstitution of Dmc1-mediated meiotic recombination. Nucleic Acids Res. 2019 Jan 25; 47(2):747–61. https://doi.org/10.1093/nar/gky1160 PMID: 30462332

61. Bishop DK. RecA homologs Dmc1 and Rad51 interact to form multiple nuclear complexes prior to meiotic chromosome synapsis. Cell. 1994 Dec 16; 79(6):1081–92. https://doi.org/10.1016/0092-8674(94)90038-8 PMID: 7528104

62. Hayase A, Takagi M, Miyazaki T, Oshiumi H, Shinohara M, Shinohara A. A protein complex containing Mei5 and Sae3 promotes the assembly of the meiosis-specific RecA homolog Dmc1. Cell. 2004 Dec; 119(7):927–40. https://doi.org/10.1016/j.cell.2004.10.031 PMID: 15620352

63. Tsubouchi H, Roeder GS. The budding yeast Mei5 and Sae3 proteins act together with Dmc1 during meiotic recombination. Genetics. 2004 Nov; 168(3):1219–30. https://doi.org/10.1534/genetics.103.025700 PMID: 15579681

64. Zierhut C, Berlinger M, Rupp C, Shinohara A, Klein F. Mnd1 Is Required for Meiotic Interhomolog Repair. Curr Biol. 2004 May; 14(9):752–62. https://doi.org/10.1016/j.cub.2004.04.030 PMID: 15120066

65. Henry JM, Camahort R, Rice DA, Florens L, Swanson SK, Washburn MP, et al. Mnd1/Hop2 facilitates Dmc1-dependent interhomolog crossover formation in meiosis of budding yeast. Mol Cell Biol. 2006 Apr; 26(8):2913–23. https://doi.org/10.1128/MCB.26.8.2913-2923.2006 PMID: 16581767

66. Argunhan B, Murayama Y, Iwasaki H. The differentiated and conserved roles of Swi5-Sfr1 in homologous recombination. FEBS Lett. 2017 May 8; 591(14):2035–47. https://doi.org/10.1002/1873-3468.12656 PMID: 28423184

67. Haruta N, Kurokawa Y, Murayama Y, Akamatsu Y, Unzai S, Tsutsui Y, et al. The Swi5-Sfr1 complex stimulates Rhp51/Rad51- and Dmc1-mediated DNA strand exchange *in vitro*. Nat Struct Mol Biol. 2006 Sep; 13(9):823–30. https://doi.org/10.1038/nsmb1136 PMID: 16921379

68. Yuan J, Chen J. The role of the human SWI5-MEI5 complex in homologous recombination repair. J Biol Chem. 2011 Mar 18; 286(11):9888–93. https://doi.org/10.1074/jbc.M110.207290 PMID: 21252223

69. Su G-C, Chung C-I, Liao C-Y, Lin S-W, Tsai C-T, Huang T, et al. Enhancement of ADP release from the RAD51 presynaptic filament by the SWI5-SFR1 complex. Nucleic Acids Res. 2014 Jan; 42 (1):349–58. https://doi.org/10.1093/nar/gkt879 PMID: 24078249

70. Ferrari SR, Grubb J, Bishop DK. The Mei5-Sae3 protein complex mediates Dmc1 activity in *Saccharomyces cerevisiae*. J Biol Chem. 2009 Apr 24; 284(18):11766–70. https://doi.org/10.1074/jbc.C900023200 PMID: 19270307

71. Bugreev DV, Mazin AV. Ca^{2+} activates human homologous recombination protein Rad51 by modulating its ATPase activity. Proc Natl Acad Sci U S A. 2004 Jul 6; 101(27):9988–93. https://doi.org/10.1073/pnas.0402105101 PMID: 15226506

72. Lu C-H, Yeh H-Y, Su G-C, Ito K, Kurokawa Y, Iwasaki H, et al. Swi5-Sfr1 stimulates Rad51 recombinase filament assembly by modulating Rad51 dissociation. Proc Natl Acad Sci U S A. 2018 Oct 23; 115(43):E10059–68. https://doi.org/10.1073/pnas.1812753115 PMID: 30297419

73. McKee AH, Kleckner N. Mutations in *Saccharomyces cerevisiae* that block meiotic prophase chromosome metabolism and confer cell cycle arrest at pachytene identify two new meiosis-specific genes *SAE1* and *SAE3*. Genetics. 1997 Jul; 146(3):817–34. PMID: 9215889

74. Akamatsu Y, Tsutsui Y, Morishita T, Siddique MSP, Kurokawa Y, Ikeguchi M, et al. Fission yeast Swi5/Sfr1 and Rhp55/Rhp57 differentially regulate Rhp51-dependent recombination outcomes. EMBO J. 2007 Mar 7; 26(5):1352–62. https://doi.org/10.1038/sj.emboj.7601582 PMID: 17304215

75. Akamatsu Y, Jasin M. Role for the mammalian Swi5-Sfr1 complex in DNA strand break repair through homologous recombination. PLoS Genet. 2010 Oct 14; 6(10):e1001160. https://doi.org/10.1371/journal.pgen.1001160 PMID: 20976249

76. Tsubouchi H, Roeder GS. Budding yeast Hed1 down-regulates the mitotic recombination machinery when meiotic recombination is impaired. Genes Dev. 2006 Jul 1; 20(13):1766–75. https://doi.org/10.1101/gad.1422506 PMID: 16818607

77. Busygina V, Sehorn MG, Shi IY, Tsubouchi H, Roeder GS, Sung P. Hed1 regulates Rad51-mediated recombination via a novel mechanism. Genes Dev. 2008 Mar 15; 22(6):786–95. https://doi.org/10.1101/gad.1638708 PMID: 18347097

78. Shinohara A, Gasior S, Ogawa T, Kleckner N, Bishop DK. *Saccharomyces cerevisiae recA* homologues *RAD51* and *DMC1* have both distinct and overlapping roles in meiotic recombination. Genes Cells. 1997 Oct; 2(10):615–29. https://doi.org/10.1046/j.1365-2443.1997.1480347.x PMID: 9427283

79. Schwacha A, Kleckner N. Interhomolog bias during meiotic recombination: meiotic functions promote a highly differentiated interhomolog-only pathway. Cell. 1997 Sep 19; 90(6):1123–35. https://doi.org/10.1016/s0092-8674(00)80378-5 PMID: 9323140

80. Campbell MJ, Davis RW. On the *in vivo* function of the RecA ATPase. J Mol Biol. 1999 Feb 19; 286 (2):437–45. https://doi.org/10.1006/jmbi.1998.2457 PMID: 9973562

81. Fortin GS, Symington LS. Mutations in yeast Rad51 that partially bypass the requirement for Rad55 and Rad57 in DNA repair by increasing the stability of Rad51-DNA complexes. EMBO J. 2002 Jun 17; 21(12):3160–70. https://doi.org/10.1093/emboj/cdf293 PMID: 12065428

82. Peck R, Olsen C. Statistics: Learning from Data (AP Edition). 1st ed. Boston: Cengage Learning.

83. Gasior SL, Wong AK, Kora Y, Shinohara A, Bishop DK. Rad52 associates with RPA and functions with Rad55 and Rad57 to assemble meiotic recombination complexes. Genes Dev. 1998 Jul 15; 12 (14):2208–21. https://doi.org/10.1101/gad.12.14.2208 PMID: 9679065

84. Cao L, Alani E, Kleckner N. A pathway for generation and processing of double-strand breaks during meiotic recombination in S. cerevisiae. Cell. 1990 Jun 15; 61(6):1089–101. https://doi.org/10.1016/0092-8674(90)90072-m PMID: 2190690

85. Shinohara M, Shinohara A. Multiple pathways suppress non-allelic homologous recombination during meiosis in *Saccharomyces cerevisiae*. PLoS ONE. 2013; 8(4):e63144. https://doi.org/10.1371/journal.pone.0063144 PMID: 23646187

86. Oh SD, Jessop L, Lao JP, Allers T, Lichten M, Hunter N. Stabilization and electrophoretic analysis of meiotic recombination intermediates in *Saccharomyces cerevisiae*. Methods Mol Biol. Totowa, NJ: Humana Press; 2009; 557(Chapter 14):209–34. https://doi.org/10.1007/978-1-59745-527-5_14 PMID: 19799185

87. Hong S, Sung Y, Yu M, Lee M, Kleckner N, Kim KP. The logic and mechanism of homologous recombination partner choice. Mol Cell. 2013 Aug 22; 51(4):440–53. https://doi.org/10.1016/j.molcel.2013.08.008 PMID: 23973374

88. Lao JP, Cloud V, Huang C-C, Grubb J, Thacker D, Lee C-Y, et al. Meiotic crossover control by concerted action of Rad51-Dmc1 in homolog template bias and robust homeostatic regulation. PLoS Genet. 2013 Dec 19; 9(12):e1003978–22. https://doi.org/10.1371/journal.pgen.1003978 PMID: 24367271

89. Dresser ME, Ewing DJ, Conrad MN, Dominguez AM, Barstead R, Jiang H, et al. *DMC1* functions in a *Saccharomyces cerevisiae* meiotic pathway that is largely independent of the *RAD51* pathway. Genetics. 1997 Oct; 147(2):533–44. PMID: 9335591

90. Bishop DK. Rad51, the lead in mitotic recombinational DNA repair, plays a supporting role in budding yeast meiosis. Cell Cycle. 2012 Nov 15; 11(22):4105–6. https://doi.org/10.4161/cc.22396 PMID: 23075494

91. Masson JY, Davies AA, Hajibagheri N, Van Dyck E, Benson FE, Stasiak AZ, et al. The meiosis-specific recombinase hDmc1 forms ring structures and interacts with hRad51. EMBO J. 1999 Nov 15; 18 (22):6552–60. https://doi.org/10.1093/emboj/18.22.6552 PMID: 10562567

92. Tarsounas M, Morita T, Pearlman RE, Moens PB. RAD51 and DMC1 form mixed complexes associated with mouse meiotic chromosome cores and synaptonemal complexes. J Cell Biol. 1999 Oct 18; 147(2):207–20. https://doi.org/10.1083/jcb.147.2.207 PMID: 10525529

93. Siaud N, Dray E, Gy I, Gérard E, Takvorian N, Doutriaux M-P. Brca2 is involved in meiosis in *Arabidopsis thaliana* as suggested by its interaction with Dmc1. EMBO J. 2004 Mar 24; 23(6):1392–401. https://doi.org/10.1038/sj.emboj.7600146 PMID: 15014444

94. Shinohara M, Gasior SL, Bishop DK, Shinohara A. Tid1/Rdh54 promotes colocalization of Rad51 and Dmc1 during meiotic recombination. Proc Natl Acad Sci U S A. 2000 Sep 26; 97(20):10814–9. https://doi.org/10.1073/pnas.97.20.10814 PMID: 11005857

95. Shan Q, Bork JM, Webb BL, Inman RB, Cox MM. RecA protein filaments: end-dependent dissociation from ssDNA and stabilization by RecO and RecR proteins. J Mol Biol. 1997 Feb 7; 265(5):519–40. https://doi.org/10.1006/jmbi.1996.0748 PMID: 9048946

96. Sung P. Yeast Rad55 and Rad57 proteins form a heterodimer that functions with replication protein A to promote DNA strand exchange by Rad51 recombinase. Genes Dev. 1997 May 1; 11(9):1111–21. https://doi.org/10.1101/gad.11.9.1111 PMID: 9159392

97. Liu J, Renault L, Veaute X, Fabre F, Stahlberg H, Heyer W-D. Rad51 paralogues Rad55-Rad57 balance the antirecombinase Srs2 in Rad51 filament formation. Nature. 2011 Oct 23; 479(7372):245–8. https://doi.org/10.1038/nature10522 PMID: 22020281

98. Shinohara M, Shita-Yamaguchi E, Buerstedde JM, Shinagawa H, Ogawa H, Shinohara A. Characterization of the roles of the *Saccharomyces cerevisiae RAD54* gene and a homologue of *RAD54*, *RDH54/TID1*, in mitosis and meiosis. Genetics. 1997 Dec; 147(4):1545–56. PMID: 9409820

99. Oh SD, Lao JP, Hwang PY-H, Taylor AF, Smith GR, Hunter N. BLM ortholog, Sgs1, prevents aberrant crossing-over by suppressing formation of multichromatid joint molecules. Cell. 2007 Jul 27; 130 (2):259–72. https://doi.org/10.1016/j.cell.2007.05.035 PMID: 17662941

100. Kaur H, De Muyt A, Lichten M. Top3-Rmi1 DNA single-strand decatenase is integral to the formation and resolution of meiotic recombination intermediates. Mol Cell. 2015 Feb 19; 57(4):583–94. https://doi.org/10.1016/j.molcel.2015.01.020 PMID: 25699707

101. Tang S, Wu MKY, Zhang R, Hunter N. Pervasive and essential roles of the Top3-Rmi1 decatenase orchestrate recombination and facilitate chromosome segregation in meiosis. Mol Cell. 2015 Feb 19; 57(4):607–21. https://doi.org/10.1016/j.molcel.2015.01.021 PMID: 25699709

102. Cejka P, Plank JL, Bachrati CZ, Hickson ID, Kowalczykowski SC. Rmi1 stimulates decatenation of double Holliday junctions during dissolution by Sgs1-Top3. Nat Struct Mol Biol. 2010 Nov; 17 (11):1377–82. https://doi.org/10.1038/nsmb.1919 PMID: 20935631

103. Fasching CL, Cejka P, Kowalczykowski SC, Heyer W-D. Top3-Rmi1 dissolve Rad51-mediated D loops by a topoisomerase-based mechanism. Mol Cell. 2015 Feb 19; 57(4):595–606. https://doi.org/10.1016/j.molcel.2015.01.022 PMID: 25699708

104. Piazza A, Shah SS, Wright WD, Gore SK, Koszul R, Heyer W-D. Dynamic processing of displacement loops during recombinational DNA repair. Mol Cell. 2019 Mar 21; 73(6):1255–1266.e4. https://doi.org/10.1016/j.molcel.2019.01.005 PMID: 30737186

105. Piazza A, Wright WD, Heyer W-D. Multi-invasions are recombination byproducts that induce chromosomal rearrangements. Cell. 2017 Aug 10; 170(4):760–773.e15. https://doi.org/10.1016/j.cell.2017.06.052 PMID: 28781165

106. Piazza A, Heyer W-D. Multi-invasion-induced rearrangements as a pathway for physiological and pathological recombination. Bioessays. 2018 May; 40(5):e1700249. https://doi.org/10.1002/bies.201700249 PMID: 29578583

107. Oh SD, Lao JP, Taylor AF, Smith GR, Hunter N. RecQ helicase, Sgs1, and XPF family endonuclease, Mus81-Mms4, resolve aberrant joint molecules during meiotic recombination. Mol Cell. 2008 Aug 8; 31(3):324–36. https://doi.org/10.1016/j.molcel.2008.07.006 PMID: 18691965

108. Jessop L, Lichten M. Mus81/Mms4 endonuclease and Sgs1 helicase collaborate to ensure proper recombination intermediate metabolism during meiosis. Mol Cell. 2008 Aug 8; 31(3):313–23. https://doi.org/10.1016/j.molcel.2008.05.021 PMID: 18691964

109. De Muyt A, Jessop L, Kolar E, Sourirajan A, Chen J, Dayani Y, et al. BLM helicase ortholog Sgs1 is a central regulator of meiotic recombination intermediate metabolism. Mol Cell. 2012 Apr 13; 46(1):43–53. https://doi.org/10.1016/j.molcel.2012.02.020 PMID: 22500736

110. Piazza A, Heyer W-D. Moving forward one step back at a time: reversibility during homologous recombination. Curr Genet. 2019 May 23:1–8.

111. Forget AL, Kowalczykowski SC. Single-molecule imaging of DNA pairing by RecA reveals a three-dimensional homology search. Nature. 2012 Feb 5; 482(7385):423–7. https://doi.org/10.1038/nature10782 PMID: 22318518

112. Wright WD, Heyer W-D. Rad54 functions as a heteroduplex DNA pump modulated by its DNA substrates and Rad51 during D-loop formation. Mol Cell. 2014 Feb 6; 53(3):420–32. https://doi.org/10.1016/j.molcel.2013.12.027 PMID: 24486020

113. Grubb J, Brown MS, Bishop DK. Surface spreading and immunostaining of yeast chromosomes. J Vis Exp. 2015 Aug 9;(102):e53081. https://doi.org/10.3791/53081 PMID: 26325523

114. Lao JP, Tang S, Hunter N. Native/Denaturing two-dimensional DNA electrophoresis and its application to the analysis of recombination intermediates. Methods Mol Biol. Totowa, NJ: Humana Press; 2013; 1054(Pt 2):105–20.

115. Arora C, Kee K, Maleki S, Keeney S. Antiviral protein Ski8 is a direct partner of Spo11 in meiotic DNA break formation, independent of its cytoplasmic role in RNA metabolism. Mol Cell. 2004 Feb 27; 13(4):549–59. https://doi.org/10.1016/s1097-2765(04)00063-2 PMID: 14992724

116. James P, Halladay J, Craig EA. Genomic libraries and a host strain designed for highly efficient two-hybrid selection in yeast. Genetics. 1996 Dec; 144(4):1425–36. PMID: 8978031